Whole-rock and zircon evidence for evolution of the Late Jurassic high Sr/Y Zhoujiapuzi granite, Liaodong Peninsula, North China Craton

Renyu Zeng [a, b,c] *, Mark B. Allen [c], Xiancheng Mao [d], Jianqing Lai [d], Jie Yan [a, b], Jianjun Wan[a, b]

[a] State Key Laboratory of Nuclear Resources and Environment, East China University of Technology, Nanchang, 330013, Jiangxi, China;

[b] School of Earth Sciences, East China University of Technology, Nanchang, 330013, China,

[c] Department of Earth Sciences, Durham University, Durham DH1 3LE, UK

[d] School of Geosciences and Info-Physics, Central South University, Changsha 410083, China

Abstract: Middle-Late Jurassic high Sr/Y granitic intrusions are extensively exposed in the Liaodong Peninsula, in the eastern part of the North China Craton (NCC). However, the genesis of the high Sr/Y signature in these intrusions has not been studied in detail. In this study, we report results of zircon U-Pb dating, Hf isotopic analysis and zircon and whole-rock geochemical data for the Late Jurassic Zhoujiapuzi granite in the middle part of the Liaodong Peninsula. The Zhoujiapuzi granite is high-K (calc-alkaline) and peraluminous in nature, with high SiO_2 (68.1–73.0 wt %) and Al_2O_3 (14.5–16.8 wt %), low in TFe_2O_3 (1.10–2.49 wt %) and MgO (0.10–0.44 wt %), and

with high Sr/Y (19.9–102.0) and La_N/Yb_N (14.59–80.40), characteristic of high Sr/Y I-type granite. The geochemical signatures, in combination with the presence of a large number of Paleoproterozoic inherited zircons, indicate that the Zhoujiapuzi granite was most likely derived from partial melting of the basement in the region, and specifically the Liaoji granites. The high Sr/Y signature is inherited from these source rocks. LA-ICP-MS zircon U-Pb dating of the autocryst zircons from two samples (from different localities) yielded consistent weighted average ages of 160.7±1.1 Ma (MSWD=1.3) and 159.6±1.1 Ma (MSWD=1.2), with εHf(t) values in the range of -26.6– -22.8. Morphological and chemical studies on autocrystic zircon grains show that there are two stages of zircon growth, interpreted as magmatic evolution in two distinct stages. The light-CL core reflects a crystallization environment of low oxygen fugacity and high T_{Zr-Ti}; the dark-CL rim formed with high oxygen fugacity and lower T_{Zr-Ti}. Based on the geochemical features and regional geological data, we propose that the Liaodong Peninsula in the Late Jurassic was part of a mature continental arc, with extensive melting of thick crust above the Paleo-Pacific subduction zone.

Keywords: Liaodong Peninsula; Late Jurassic; Zircon U-Pb-Hf isotopes; Two stages of crystal growth; High Sr/Y granite

1. Introduction

The Liaodong Peninsula is located in the northeast of the North China Craton (NCC). The northeast NCC was influenced by three main tectonic regimes in the Mesozoic, related to the subduction of the Paleo-Asian, Paleo-Pacific and Mongol-Okhotsk oceans (Tang et al., 2018). The superposition of these different regimes

resulted in changing tectonic and magmatic patterns over time. Middle-Late Jurassic granitic rocks are extensively exposed in the northern parts of the Liaodong Peninsula, such as the Yutun mylonitic granite, Xiaoheishan granodiorite, Heigou monzogranite (Wu et al., 2005), Wulong two-mica monzogranite (Yang et al., 2018), and Huangdi biotite monzogranite (Xue et al., 2020). Most of these rocks are characterized by high Sr /Y, and plot within the adakite field on Sr/Y-Y and La_N/Yb_N-Yb_N diagrams (Wu et al., 2005a; Yang et al., 2015a, 2018).

The geodynamic settings and petrogenesis of adakite and geochemically similar high Sr/Y igneous rocks have been widely discussed. The high Sr/Y rocks were originally proposed to be formed by melting of young (<25 Ma) and hot subducted oceanic slab in an arc setting (Defant and Drummond, 1990). However, later studies have shown that the high Sr/Y rocks can form in both arc and non-arc settings by other processes, such as continental interior settings (Wang et al., 2007), cold subduction zones (Nakamura and Iwamori, 2013), collision or post-collision processes (Schwartz et al., 2011). In addition, numerous studies have suggested that the lower continental crust can also be the source of the high Sr/Y rocks (Gao et al., 2004; Ou et al., 2017). However, it is debated whether crustal thickening is necessary for their formation (e.g. Moyen, 2009; Kamei et al., 2009; Zhan et al., 2020). In recent years, some studies have proposed that the high Sr/Y ratio in granitic rocks can be inherited from a high Sr/Y crust source, regardless of pressure (Kamei et al., 2009; Ma et al., 2015; Zhan et al., 2020).

The Middle-Late Jurassic granitic rocks in the Liaodong Peninsula are commonly proposed to be the products of partial melting of thickened mafic crust with garnet in the residue (Wu et al., 2005a; Yang et al., 2015a, 2018; Tang et al., 2018). However, the source composition has not been fully considered in the petrogenesis of the high Sr/Y

rocks in the Liaodong Peninsula. Hence, the petrogenesis of the Middle-Late Jurassic high Sr/Y rocks needs to be re-evaluated, based on more detailed work and a consideration of possible sources. This petrogenesis is of significance for understanding the Jurassic tectonics of the Liaodong Peninsula, and the NCC in general.

In this paper, we examined the high Sr/Y Zhoujiapuzi granite from the Xiuyan area, in the middle of the Liaodong Peninsula. Zircons are analysed for U-Pb-Hf isotopes and trace element geochemistry, and by Raman spectroscopy. These results are integrated with whole-rock geochemistry. We focus on the zircons, because of their potential to reveal the origins of the pluton (Belousova et al., 2002; Wang et al., 2007; Breiter et al., 2014; Zhao et al., 2014), and so provide a case study for the evolution of plutonic magma systems in general. Based on observations of the CL images and chemical analysis, two zircon growth stages can be distinguished. We first determine the crystallization environments of the two zircon growth stages, and then decipher the petrogenesis, source characteristics and origin of the high Sr/Y signature of the pluton as a whole. Integrated with previous studies, our study provides insights into the tectonic evolution of the Liaodong Peninsula in the Late Jurassic.

2. Geological setting

The Zhoujiapuzi granite is located in the middle of the Liaodong Peninsula, at the northeastern margin of the NCC (Fig. 1). The Paleoproterozoic Liaohe Group and Liaoji granite are the basement in the study area. The Liaohe Group includes the Lieryu, Gaojiayu, Dashiqiao and Gaixian formations. Although stratigraphic terms are used, these rocks are metamorphic, and the group consists of leptynite, leptite, granulite, amphibolite, marble and phyllite. The protoliths of the Liaohe Group include marine

volcanics, clastics, carbonates and claystones. The formation age of the metasedimentary rocks in the Liaohe Group is 2.0–1.9 Ga (Wan et al., 2006; Li et al., 2015). It is in unconformable contact with the overlying strata of the Mesoproterozoic Cuocaogou Formation and Xiaoling Formation.

The study area experienced strong magmatic activity in the Paleoproterozoic, which can be divided into two stages of 2.2–2.1 Ga and ~ 1.85 Ga. The 2.18–2.14 Ga Liaoji granites (also called gneissic granites), which lie within an area measuring 300 km × 70 km, are dominated by A- and I-type granites (Li and Zhao, 2007; Yang et al., 2016; Wang et al., 2020a). Metamorphosed volcanic rocks (leptynite, leptite and granulite) in the Liaohe Group also formed at 2.2–2.1 Ga (Li et al., 2015). The ~1.85 Ga granites mainly consist of I- and S-type porphyry granites and alkaline syenites (Yang et al., 2007; Yang et al., 2015b). In addition, there were small amounts of mafic magmatic activity at ~2.17 Ga, ~2.1 Ga and ~1.8 Ga (Meng et al., 2014; Yuan et al., 2015). There are a variety of viewpoints on the Paleoproterozoic tectono-magmatic evolution in the Liaodong Peninsula, such as an intracontinental rift opening-closing model (Li et al., 2005) and an arc-continent collision model (Faure et al., 2004).

In the Mesozoic, the region of the Liaodong Peninsula was influenced by the circum-Pacific tectonic regime, the Mongol-Okhotsk tectonic regime and the Paleo-Asian Ocean tectonic regime. The joint influence of multiple tectonic regimes resulted in intensive magmatism during the Mesozoic (Fig. 1b). These Mesozoic magmatic rocks can be divided into three stages, namely: Triassic (233–212 Ma), Jurassic (180–156 Ma) and Early Cretaceous (131–117 Ma) (Wu et al., 2005b).

The Triassic magmatic rocks are less exposed, mainly alkaline rocks, diabase, diorites and granites (Wu et al., 2005b). Among them, the granites mainly have A-type affinity, and may have formed in an extensional setting (Tang et al., 2018; Wang et al., 2019). Magmatism has been related to either the subduction of the Paleo-Pacific slab, closure of the Paleo-Asian Ocean, or the collision between the NCC and the Yangtze Craton (Tang et al., 2018; Wang et al., 2019). The majority of the Jurassic magmatic rocks are monzogranite and granodiorite, which are generally calc-alkaline I-type granites, and show characteristics of adakite-like rocks. Some of them, exposed near later extensional structures, have undergone regional ductile deformation. These Jurassic magmatic rocks are generally considered to relate to the subduction of the Paleo-Pacific slab (Wu et al., 2005a; Zhai et al., 2004). In the Early Cretaceous, basic-acidic-alkaline rocks were widely developed. Among them, the granites have mainly A- and I-type affinities. These rocks are generally considered to have formed in an intense extensional environment, which is connected with either the rollback or low-angle subduction of the Paleo-Pacific slab (Wu et al., 2005c; Zheng et al., 2018).

3. Samples and petrography

The Zhoujiapuzi granite is located to the east of Xiuyan City, in the middle of the Liaodong Peninsula (Fig. 1b). It intruded into the Lieryu Formation of the Liaohe Group. Eight samples of the Zhoujiapuzi granite were collected at locations shown in Fig. 1c.

The Zhoujiapuzi granite is generally grey in colour and with fine-grained texture (Fig. 2a). The mineral assemblage contains K-feldspar (~50 %), quartz (~25 %),

plagioclase (~20 %) and biotite (~5 %) as well as accessory minerals such as zircon,

ilmenite, magnetite and apatite. K-feldspar grains are euhedral or subhedral, and always

exhibit cross-hatched twinning (Fig. 2b). Quartz grains are usually xenomorphic, and

have indented boundaries and wavy extinction (Fig. 2b-d). Plagioclase always exhibits

polysynthetic twinning and have sericitization in places (Fig. 2c). Biotite mainly fills

in the interstices between the other minerals (Fig. 2c, d).

4. Analytical methods

The cathodoluminescence (CL) images of zircon were obtained by the Chengpu

geological Testing Co. Ltd, Langfang, China using the TIMA analysis. The LA-ICP-

MS zircon U-Pb analyses were performedusing an Agilent Technologies 7700x ICP-

MS with a Teledyne Cetac Technologies Analyte Excite laser-ablation system at

Nanjing FocuMS Contract Testing Co. Ltd. The analyses were carried out with a 35 μm

spot size at 8 Hz repetition rate for 40 seconds. The ICP-MS detector has dual modes:

pulse for lower signal, and analog for higher signal. Pulse-analog cross calibration was

performed before the measurement of U-Pb isotopes, delivering a wider linear dynamic

range – up to 10 orders of magnitude. For a signal of ^{238}U higher than 1.2–1.4 Mio cps,

equivalent zircon contains U concentrations higher than 600 ppm, and are measured in

analog mode. 91500 was used as external standard. GJ-1 (600Ma, Jackson et al., 2004)

and Plešovice (337Ma, Sláma et al., 2008) were treated as quality control for

geochronology. During our analyses, the weighted mean age of GJ-1 and Plešovice

were 606.0 ± 4.8 Ma (n=16, MSWD = 0.50) and 340.9 ± 4.0 Ma (n=7, MSWD = 1.0),

respectively. Trace elements abundance of zircon were externally calibrated against

NIST SRM 610 with Si as the internal standard. The raw ICP-MS data were processed

using ICPMSDataCal software (Liu et al., 2010). No common-Pb correction was applied to the data. Data reduction was completed using the Isoplot4.15 (Ludwig, 2003). The instrument description and analytical procedure are described in detail by Zeng et al. (2018).

The in-situ Lu-Hf isotopic analyses of zircon were performed by LA-MC-ICP-MS using a Teledyne Cetac laser-ablation system and a Nu Plasma II MC-ICP-MS at Nanjing FocuMS Contract Testing Co. Ltd. The 193 nm ArF excimer laser was focused on zircon surface with fluence of 6.0J/cm^2. The ablation protocol employed a spot diameter of 50 um at 8 Hz repetition rate for 40 seconds. Three standard zircons, GJ-1, 91500, and Penglai, were analysed for quality control at every ten unknown samples. In the experiment, standard zircon GJ-1, 91500, and Penglai were analyzed, and the $^{176}Hf/^{177}Hf$ ratios were 0.282002–0.282013, 0.282305–0.282315 and 0.282901–0.282914 respectively, in accordance with their recommended values (GJ-1: 0.282012, Yuan et al., 2008; 91500: 0.282307 ± 0.000031, Wu et al., 2006; Penglai: 0.282906 ± 0.000010, Li et al., 2010). For the calculation of $\varepsilon Hf(t)$ values, we have adopted the ^{176}Lu decay constant of 1.867×10^{-11} (Söderlund et al., 2004), the present-day chondritic values of $^{176}Lu/^{177}Hf = 0.0332$ and $^{176}Hf/^{177}Hf = 0.282772$ (Blichert-Toft and Albarède 1997). To calculate one-stage model ages (T_{DM1}) relative to a depleted-mantle source, we have adopted the present-day depleted-mantle values of $^{176}Lu/^{177}Hf = 0.0384$ and $^{176}Hf/^{177}Hf = 0.28325$ (Vervoort and Blichert-Toft 1999). To calculate two-stage modal ages (TDM2), 'felsic crust' model ages are calculated using average continental crust $^{176}Lu/^{177}Hf = 0.015$ (Griffin et al., 2004).

182   Zircon Raman analyses were carried out using an RM2000 laser Raman

183   spectrometer at the State Key Laboratory of Nuclear Resources and Environment, East

184   China University of Technology. The selected incident wavelengths were 532 and 785

185   nm in order to clearly identify the luminescence bands due to low concentration

186   impurities. The beam power was 20 mW. The Leica 50× objective was employed.

187   Six fresh rock samples were selected for geochemical analysis. The elemental

188   analyses were conducted at Analytical Chemistry & Testing Services (ALS) Chemex

189   (Guangzhou) Ltd. Major oxides were analyzed using wave-dispersive X-ray

190   fluorescence (XRF) (ME-XRF26). Analytical precision was better than $\pm$ 0.01%.

191   Trace element abundances were measured by the lithium borate dissolution method and

192   ICP-MS (ME-MS81). The analytical uncertainties of the rare earth element (REE) and

193   high field strength element (HFSE) are <5%. Analytical uncertainties are in the range

194   of 5%–10% for the other elements. Detailed analytical procedures refer to Zhang et al.

195   (2019) and Nash et al. (2020).

196   **5. Analytical results**

197   The data for major and trace elements, Raman microprobe data, zircon trace

198   elements, zircon U-Pb ages, and zircon Hf isotopes are shown in Tables S1, S2, S3, S4

199   and S5, respectively.

200   **5.1. Whole-rock major and trace element compositions**

201   SiO$_2$ contents range from 68.11 wt.% to 73.02 wt.% (average 71.71 wt.%).

202   Contents of Na$_2$O and K$_2$O are 3.81－4.65 wt.% and 4.32－4.71 wt.%, respectively,

203   with Na_2O/K_2O ratio of 0.82－1.08 and total alkalis ($Na_2O + K_2O$) of 8.38－8.97. All

204   samples plot in the field of granite in the TAS classification except one (Fig. 3a). These

205   samples have Al_2O_3 contents of 14.49－16.83 wt.% (average 15.09 wt.%), CaO

206   contents of 1.04－1.98 wt.% (average 1.38 wt.%) and A/CNK values of 1.05－1.10

207   (average 1.07). In the A/NK－A/CNK diagram (Fig. 3b), all samples plot in the

208   peraluminous field (Fig. 3b). The granite samples have low TFe_2O_3 (TFe_2O_3 = all Fe

209   calculated as Fe_2O_3) contents and MgO contents ranging from 1.10–2.49 wt % and

210   0.10–0.44 wt %, respectively, with Mg# (Mg#=100*molar Mg/(Mg+Fe)) values of 15–

211   26.

212   The samples of the Zhoujiapuzi granite exhibit variable REEs, with total REEs

213   ranging from 59 to 302 ppm. The La_N/Yb_N values of the Zhoujiapuzi granite range from

214   14.59 to 80.40 (average 38.27), showing right-declined REE patterns (Fig. 4a). The

215   samples have Eu/Eu* of 0.62–1.94 and Ce/Ce* of 0.94–1.16. In the primitive mantle-

216   normalized trace element diagram (Fig. 4b), the samples show negative anomalies of

217   HFSEs (e.g., Nb, Ta, Ti and P) and positive anomalies of La and LILEs (e.g., K, Rb,

218   Ba, U, La, Ce). The Zhoujiapuzi granite is characterized by high contents of Sr (309–

219   551 ppm) and low contents of Y (5.01–15.5 ppm) and Yb (0.43–1.40 ppm), with high

220   Sr/Y ratios of 19.94–102.04 (average 65.50).

221   **5.2 Zircon CL images, Raman spectra and REE elements**

222   CL images of zircons from the Zhoujiapuzi granite are shown in Fig. 5. Zircons

223   commonly have crystal sizes between 150 and 250 μm, and have length/width ratios of

224   2:1–4:1, with euhedral, stubby to elongate prisms. According to the CL images, most

225   zircons show an internal division into 2 distinct domains: light-CL core and dark-CL

rim. The light-CL core is characterized by bright CL intensity and widely-spaced oscillatory zoning patterns. The dark-CL rim is overgrown continuously by the light-CL core and is characterized by extremely low CL emission and narrowly-spaced oscillatory zoning patterns. In addition, some zircons have inherited cores, which have corroded and rounded shapes in contact with the light-CL core, such as 1# and 37# in XY-001 and 6# and 41# in XY-008 (Fig. 5). These inherited zircons have oscillatory zoning in CL images.

Six light-CL core spots and six dark-CL rim spots were analyzed for Raman spectra. The light-CL cores have antisymmetric stretching vibration (B_{1g}) of the SiO_4 tetrahedra (v_3 (SiO_4)) Raman band of 1005–1007 cm^{-1} and half-width of the v_3 (SiO_4) Raman band (b) values of 6.0–8.1 cm^{-1}, while the dark-CL rims have v_3 (SiO_4) Raman band of 1004–1007 cm^{-1} and b values of 5.4–9.0 cm^{-1}.

Twenty light-CL core spots, eighteen dark-CL rim spots and six inherited zircon spots were analyzed for trace and rare earth elements. The light-CL core spots have lower U content (28–677 ppm) than the dark-CL rim spots (U=641–3842 ppm). In the chondrite-normalized REE element diagram (Fig. 6a, b), both the light-CL core and dark-CL rim are characterized by HREE enrichment relative to LREE with positive Ce anomalies and negative Eu anomalies. The light-CL core spots have ΣREE of 49–1115 ppm (average 390 ppm), ΣLREE of 3–72 ppm (average 14 ppm) and ΣHREE of 46–1100 ppm (average 377 ppm), whereas the dark-CL rim spots have ΣREE of 327–1632 ppm (average 895 ppm), ΣLREE of 2–14 ppm (average 6 ppm) and ΣHREE of 325–1627 ppm (average 889 ppm). Hence, the REE content of the light-CL core is significantly lower than that of the dark-CL rim, and the difference between the two is mainly in HREE content. The light-CL core spots have Eu/Eu* of 0.07–0.60 (average

251 0.28) and Ce/Ce* of 1.89–24.27 (average 10.03). Because the contents of La and Pr are

252 typically present very low, Ce* in this study is obtained by the formulation $(Nd_N)^2/Sm_N$

253 (Loader et al., 2017). The dark-CL rim spots have Eu/Eu* of 0.08–0.24 (average 0.13)

254 and Ce/Ce* of 6.57–200.31 (average 79.23). These results indicate that the light-CL

255 core have a weaker negative Eu anomaly and a weaker positive Ce anomaly than those

256 of the dark-CL rim. The inherited zircon spots have ΣREE of 602–1517 ppm, and show

257 depletion of LREE, enrichment of HREE, a positive Ce anomaly (Ce/Ce* of 1.52–

258 216.08) and a negative Eu anomaly (Eu/Eu* of 0.07–0.13) (Fig. 6c).

259 **5.3 Zircon U–Pb and Hf isotope composition**

260 Seventy-seven spots were analysed for U-Pb isotope composition from samples

261 XY-001 and XY-008. In the U-Pb Concordia diagram (Fig. 7a, c), both the light-CL

262 core and dark-CL rim spots overlap within uncertainty on the Concordia curve. There

263 is a large degree of overlap between the dark-CL rim and light-CL core in terms of

264 $^{206}Pb/^{238}U$ age although the mean value for $^{206}Pb/^{238}U$ age is higher in the light-CL core

265 (Fig. 7e). On a single zircon, the $^{206}Pb/^{238}U$ age of the light-CL core is older than that

266 of the dark-CL rim (Fig. 5). In sample XY-001, 33 spots define a weighted mean

267 $^{206}Pb/^{238}U$ age of 160.7±1.1 Ma (2σ, MSWD=1.3; Fig. 7b). In sample XY-008, 28 spots

268 define a weighted mean $^{206}Pb/^{238}U$ age of 159.6±1.1 Ma (2σ, MSWD=1.2; Fig. 7d). The

269 other 10 spots with distinctly older ages ($^{207}Pb/^{206}Pb$ ages ranging from 2500 to 2173

270 Ma) were obtained on inherited cores. Their ages are discordant, suggesting that these

271 inherited cores were variably influenced by lead loss. Among these, 9 spots define a

272 discordia line with an upper intercept age of 2163 ± 13 Ma (MSWD=0.45) (Fig. 7f).

273 Twenty-four zircons were analyzed for Lu-Hf isotope composition. The variation

274 in Hf isotopic data is limited, between 9 spots from light-CL core and 9 spots from dark-

275   CL rim. 18 spots exhibit a range of ^{176}Hf/^{177}Hf ratios from 0.281921 to 0.282030, which

276   converts to εHf(t) values between -26.6 to -22.8 (Fig. 8), and two-stage Hf model (T$_{DM2}$)

277   ages of 2650 to 2889 Ma by using the U-Pb age for each zircon. Six analytical spots,

278   which define the Concordia upper intercept age of 2163 Ma, show ^{176}Hf/^{177}Hf radios

279   and εHf(t) values of 0.281443 to 0.281496 and -0.7 to 1.5, respectively, with T$_{DM2}$ age

280   of 2648 Ma to 2791 Ma by using the upper intercept age.

281   **6. Discussion**

282   **6.1 Significance of the two stages of zircon**

283   Generally, zircon with high U content can easily break down into the metamict

284   state because of the radiation damage to the lattice caused by α-particles originating

285   from the decay of uranium (Mezger and Krogstad, 1997). The physical and structural

286   changes often lead to the loss of Pb and addition of trace elements such as LREE. In

287   this study, the dark-CL rim spots have high U content, which is significantly higher than

288   the median value of zircon U content in granitic magma (350 ppm, Wang et al., 2011).

289   Hence, the metamictization degree of the zircons must be taken into consideration. Data

290   from dark-CL rim spots plot on the Concordia curve, indicating no obvious Pb loss. The

291   internal structure of dark-CL rim is relatively intact, with obvious oscillatory zoning,

292   and few cracks, implying that the physical and structural of the dark-CL rim remained

293   unchanged. Nasdala et al. (1998) suggested that the metamictization of zircon can be

294   well characterized by Raman spectroscopy. The half-width of the v_3(SiO$_4$) Raman band

295   (*b*) of 10 cm^{-1} and 20 cm^{-1} are proposed to approximately distinguish well-crystallized,

296 intermediate and metamict zircons (Nasdala et al., 1998). The dark-CL rim have b

297 values of 5.4–9.2, characterizing them as well-crystallized. Therefore, the above

298 features indicate that the dark-CL rim are not metamict. Consequently, it can be

299 concluded that the U-Pb isotope and trace element systematics of the dark-CL rim have

300 not been changed by metamictization.

301   Both the light-CL core and dark-CL rim have oscillatory zoning patterns, and their

302 chondrite-normalized REE patterns are characterized by steeply positive slopes from

303 the LREE to HREE with strong negative Eu anomalies and pronounced positive Ce

304 anomalies. The above characteristics are consistent with those of igneous zircon

305 (Hoskin and Schaltegger, 2003). Although hydrothermal zircon can also have

306 oscillatory zoning patterns similar to magmatic zircons, there are obvious differences

307 in trace elements between the magmatic and hydrothermal zircon (Hoskin et al., 2005).

308 In the discrimination diagram (Fig. 9), both the spots of light-CL core and dark-CL rim

309 fall in or near the magmatic field, which is obviously different from hydrothermal

310 zircon. Hence, the above characteristics indicate that both the light-CL core and dark-

311 CL rim have a magmatic origin.

312   The light-CL core was overgrown continuously by the dark-CL rim. In addition,

313 the contact between the light-CL core and dark-CL rim is euhedral. Such core-mantle

314 overgrowth relationships indicate that the light-CL core domains are not inherited

315 zircons. The similar Hf isotopic data of the light-CL core and dark-CL rim is also

316 consistent with this interpretation. For the age population, the samples of XY-001 and

317 XY-008 have MSWD of 1.3 and 1.2, respectively, which are both within the expected

318 range for 95 % confidence interval (Mahon, 1996). Although the $^{206}Pb/^{238}U$ age of dark-

319 CL rim is generally younger than that of light-CL core, the ages of these two distinct

320 domains have the characteristics of continuous variation, and do not show two or more

321 distinct age populations (Fig. 7b, d). These phenomena do not support the presence of

322 antecrystic zircons (Siégel et al., 2018). Hence, both the light-CL core and dark-CL rim

323 are most likely autocrystic zircon formed in one distinct pulse of magma. The weighted

324 mean U-Pb ages of 160.7±1.1 Ma and 159.6±1.1 Ma can be interpreted as the

325 emplacement age of the Zhoujiapuzi granite. The obvious difference in internal

326 structure and trace element composition between the light-CL core and dark-CL rim

327 could be due to significant changes in their crystallization environments (Wang et al.,

328 2007).

329 The Zr/Hf ratio in zircon has a negative correlation with the degree of fractionation

330 in the parent melt (Claiborne et al., 2006). In this study, the Zr/Hf ratios of the dark-CL

331 rim (21–40) are obviously lower than those of the light-CL core (39–56) (Fig. 10a). In

332 addition, incompatible elements such as U and REE will become enriched in the highly

333 evolved magma (Zhao et al., 2014). In this study, the contents of U and REE of dark-

334 CL rim are significantly higher than those of light-CL core (Fig. 10a). Overall, the

335 above features reflect that the dark-CL rim crystallized from a later and more evolved

336 magma.

337

338 Watson and Harrison (2005) found that the Ti content of zircon has a strong

339 dependence on temperature (T), and obtained a Ti-in-zircon thermometer (T_{Zr-Ti}). Since

340 then, Ferry and Watson (2007) suggested that the solubility of Ti in zircon depends not

341 only on T and activity of TiO_2 ($aTiO_2$) but also on the activity of SiO_2 ($aSiO_2$), and

342 revised the T_{Zr-Ti}. We use the T_{Zr-Ti} from Ferry and Watson (2007) and the recommended

343 values ($aSiO_2=1$, $aTiO_2 = 0.5$) for the activity of SiO_2 and TiO_2 (Schiller and Finger,

344 2019), due to the presence of ilmenite and quartz in the Zhoujiapuzi granite. The T_{Zr-Ti}

345 from the light-CL core and dark-CL rim are 684–830 °C (average 761 °C) and 509–

346 712°C (average 635 °C), respectively, i.e. the light-CL core formed at higher

347 temperatures than the dark-CL rim. The T_{Zr-Ti} value shows a significant positive

348 correlation with Zr/Hf (a tracer of fractional crystallisation), and shows continual

349 fractionation and cooling (Fig. 10b). As the light-CL core and dark-CL rim formed in

350 different magmatic evolution stages, it is problematic to use the same $aSiO_2$ and $aTiO_2$

351 values to calculate both T_{Zr-Ti} values for both. For ilmenite bearing granites, Schiller

352 and Finger (2019) suggested that the variation of $aTiO_2$ values corresponding to

353 different zircon crystallization stages is small. In addition, Schiller and Finger (2019)

354 showed that the $aSiO_2$ value of the ilmenite-bearing granites at the onset of magmatic

355 zircon crystallization was more than 0.75. Even if the $aSiO_2$ value of the light-CL core

356 is changed from 1.0 to 0.75, the temperature will only drop by about ~27 ℃, which is

357 significantly lower than the 126 °C difference between the average T_{Zr-Ti} value of the

358 light-CL core and dark-CL rim. Therefore, it is certain that the light-CL core formed at

359 higher temperatures than the dark-CL rim, although we cannot calculate the specific

360 temperature difference.

361

362   Cerium exists in magmas as both Ce^{3+} and Ce^{4+}. Because the 0.84-Å radius of the

363   Zr^{4+} ion is more closely matched by the Ce^{4+} (0.97-Å radius) than the Ce^{3+} (1.143-Å

364   radius) (all ionic radii are from Shannon, 1976), Ce^{4+} is more compatible in the zircon

365   structure than the Ce^{3+}. Hence, the magnitude of Ce anomaly is a useful tool for

366   evaluating the oxygen fugacity condition of crystallization environment (e.g. Ballard et

367   al., 2002; Trail et al., 2012). Loader et al. (2017) suggested that the Ce/Ce* ratio is

368   likely to be the most robust measure of magma redox conditions, although it is only a

369   semi-quantitative measure. In this study, the Ce/Ce*ratio of the light-CL core and dark-

370   CL rim are 6.30–153.36 (average 32.51) and 21.81–5773.06 (average 787.39),

371   respectively. This result suggests that the dark-CL rim formed in a higher oxygen

372   fugacity environment than the light-CL core. As shown in the Ce/Ce*-Zr/Hf diagram

373   (Fig. 10c), Ce/Ce* has a significant negative correlation with Zr/Hf, showing that the

374   oxygen fugacity condition is increasing with the evolution of magma.

375

376   The absence of enclaves and disequilibrium textures in the Zhoujiapuzi granite

377   and uniform εHf(t) values of the light-CL core and dark-CL rim do not support magma

378   mixing and wall-rock assimilation. Consequently, the abrupt change between the

379   crystallization environment of the light-CL core and dark-CL rim is not due to the

380   magma mixing or contamination during magma evolution. Therefore, we propose that

381   the light-CL core was formed in a relatively deep magma chamber, which had low

382   oxygen fugacity, low Zr saturation and higher temperature. The low Th, U and REE,

383   and widely-spaced oscillatory zoning patterns indicate a low growth rate of zircon

(Hoskin and Schaltegger, 2003; Wang et al., 2011). In contrast, the dark-CL rim was formed during the ascent and/or at the emplacement location of the magma. At this stage, the oxygen fugacity significantly increased, the temperature decreased, and Zr saturation increased due to the crystallization differentiation. In this environment, the crystallization rate of zircon significantly increased, forming the zircons with a higher content of Th, U and REE elements, low CL emission and narrowly-spaced oscillatory zoning patterns.

Zircon U-Pb dating is the most commonly used method in geochronology, especially dating the emplacement age of magmatic rocks. A weighted mean age or upper intercept age is usually obtained to represent the emplacement time of a magmatic rock. However, the autocrystic zircons in this study record two different magmatic evolution stages. Previous studies, such as Wang et al. (2007), Zhao et al. (2014) and Chen et al. (2020), also show that zircons can crystallize continually or intermittently in a single phase of magmatism, showing several growth zones of clearly different internal structure and distinct time difference. Therefore, autocrystic zircon can be formed in two or more evolution stages during one distinct pulse or increment of magma. Some scholars even regard that the age difference of different stages can be more than dozens of Ma (Wang et al., 2007). Therefore, if the zircon ages in the same magmatic rock have a large range of variation, this could be caused by the zircons recording different stages in magmatic evolution, related to different levels of magma within the crust and/or different temperature regimes. In this paper, although the apparent age of the dark-CL rim is generally younger than that of the light-CL core, the

age difference between the two is within the error range of the in-situ LA-ICP-MS analyses (individual spot of $\pm$3–5% relative precision, Schmitz and Kuiper, 2013). Therefore, further work is needed to verify the actual age difference between the two magmatic evolution stages. Nevertheless, it is notable that the bulk petrology and geochemistry of the host pluton does not record and reveal this two-stage magmatic evolution, which can only be detected in the zircon analysis.

6.2 Genetic type: I-type affinity

The Zhoujiapuzi granite has low Zr (113－242 ppm), Ce (26.5－121.5 ppm), Zr+Nb+Ce+Y (152.0－382.6 ppm), $(Na_2O + K_2O)/CaO$ (4.53－8.31) and FeO^*/MgO (5.09－10.56), distinct from the typical A-type granites (Fig. 11a-d). Furthermore, the Zhoujiapuzi granite does not contain mafic alkaline minerals, such as arfvedsonite, riebeckite, etc., which is also distinctly inconsistent with typical A-type granites (Wu et al., 2003). Wu et al. (2017) suggested that a high formation temperature is one of the most important characteristics of A-type granite. Zircon saturation thermometry (T_{Zrn}) and Ti-in-zircon thermometer (T_{Zr-Ti}) are two methods for estimating magma temperatures. As noted above, because the values of aSiO$_2$ and aTiO$_2$ during the early zircon crystallization cannot be accurately obtained, the temperature of this period cannot be accurately obtained through the Ti-in-zircon thermometer. Zircon saturation thermometry was introduced by Watson and Harrison (1983) and is suitable for non-peralkaline crustal source rocks. Since the zircon solubility is mainly affected by temperature, major element compositions have a limited impact on calculated T_{Zrn}

(Miller et al., 2003). In addition, the errors introduced by crystal-rich composition tend to cancel as changes in Zr concentration and M value during crystallization have opposite effects on the T_{Zrn} value (Miller et al., 2003). Therefore, the composition of Zhoujiapuzi granite can be used to estimate the magma temperature. The calculated T_{Zrn} values for the Zhoujiapuzi granite are in the range of 803-870 °C (mean=845 ±20°C). It was proposed that the T_{Zrn} suggests an upper limit on the temperature of melt generation for inheritance-rich granitoid (Miller et al., 2003). Hence, the magma temperature of the Zhoujiapuzi granite should be lower than or equal to the T_{Zrn} value, which is significantly lower than that of typical A-type granite (>900 ℃, Skjerlie and Johnston, 1992; Douce, 1997). Thus, the Zhoujiapuzi granite is not an A-type granite.

The samples of the Zhoujiapuzi granite have A/KNC < 1.1, relatively high Na_2O (3.96–4.65 wt.%) and lack peraluminous minerals (e.g. cordierite, andalusite, muscovite and garnet), which are clearly different from S-type granites (Chappell and White, 1992). With the rise of the degree of crystallization, P_2O_5 contents (generally>0.1 wt.%) increase in S-type granites, accompanied by an increase/immutability in SiO_2 (Wolf and London, 1994). However, the Zhoujiapuzi granite samples have low P_2O_5 contents (0.02 – 0.08 wt.%), and decrease with increasing SiO_2 (Fig. 11e), which are features consistent with the I-type granite rather than S-type granite (Chappell and White, 1992). Additionally, Rb has a positive correlation with Y (Fig. 11f), which has been considered as an indicator of I-type granite (Jiang et al., 2018). Furthermore, the composition of the Zhoujiapuzi granite fall in the

I-type granite field in the discrimination diagrams of granites introduced by Collins et al. (1982) (Fig. 11 c-d). Therefore, we conclude that the Zhoujiapuzi granite is a I-type granite.

6.3 Petrogenesis of the high Sr/Y granite

The samples of the Zhoujiapuzi granite have high Sr/Y and $(La/Yb)_N$ ratios and low Y and Yb contents (Fig. 12a) consistent with the geochemical signatures of modern adakites (Defant and Drummond, 1990). However, other geochemical parameters of the Zhoujiapuzi granite, such as the high K_2O/Na_2O ratio (0.93 –1.22), low Al_2O_3 content (14.49 –15.02%, except one) and Sr content (in half of the samples lower than 400 ppm), are obviously different from typical adakites ($K_2O/Na_2O \leqslant 0.42$, $Al_2O_3 \geqslant$ 15 %, Sr>400 ppm, Defant and Drummond., 1990; Drummond et al., 1996, Martin et al., 2005). A variety of petrogenetic models have been proposed for the origin of high Sr/Y magmatic rocks, such as partial melting of subducting oceanic crust (Model A, Defant and Drummond, 1990), delaminated lower continental crust (LCC) (Model B, Kay and Kay, 1993; Xu et al., 2002), differentiation of basaltic arc magma (Model C, Castillo et al., 1999), magma mixing between mantle-derived mafic and crust-derived silicic magmas (Model D, Ma et al., 2013a), partial melting of thickened basaltic LCC (Model E, Gao et al., 2004; Ou et al., 2017), or melting of a high Sr/Y (and La/Yb) source (Model F, Kamei et al., 2009; Ma et al., 2015).

6.3.1 Model A: Partial melting of subducting oceanic crust

The partial melting of the young, hot and hydrated subducted oceanic slab in the garnet stability field is the classical formation model of adakite (high Sr/Y rock) (Defant and Drummond, 1990). Studies have shown that the rock with this genetic model

472 generally has the characteristics of high mantle components (such as MgO, CaO and

473 Cr) because of the involvement of mantle magma (Wang et al., 2018). However, this

474 phenomenon was not seen in the Zhoujiapuzi granite. In addition, the Zhoujiapuzi

475 granite has high K_2O/Na_2O ratios (0.92–1.22, average 1.13), which is inconsistent with

476 the slab-derived adakites (K_2O/Na_2O= ~0.4, Martin et al., 2005). Moreover, the low

477 εHf(t) values (-26.6 to -22.8) of the Zhoujiapuzi granite are also inconsistent with the

478 magmas derived from the partial melting of oceanic crust, which generally have

479 depleted isotopic character (Zhan et al., 2020). Furthermore, the Zhoujiapuzi granite

480 has low Ti/Eu and high Nd/Sm radios (Fig. 13a), and markedly negative Nb-Ta

481 anomalies (Fig. 4b), which are distinct from those of oceanic basalts (Yu et al., 2012).

482 In summary, the Zhoujiapuzi granite is difficult to explain by Model A.

6.3.2 Model B: Delaminated lower continental crust (LCC)

484 High-density, garnet-bearing mafic lower crust delaminating or foundering into

485 the asthenosphere mantle and subsequent interaction with mantle peridotite could

486 produce high Sr/Y magmas (Kay and Kay 1993). Because the melt formed by partial

487 melting of the delaminated lower crust would interact with mantle peridotite during

488 magma ascent, the high Sr/Y magmas related to this petrogenetic model generally have

489 high MgO, Mg# and TiO_2 (Gao et al., 2004; Ou et al., 2017; He et al., 2021). The MgO

490 (0.10– 0.44 wt.%), Mg# (15– 26) and TiO_2 (0.09– 0.34 wt.%) values of Zhoujiapuzi

491 granite are significantly lower than the above values (Fig. 13b- d). In addition,

492 delamination of the lower crust generally occurs in within-plate extensional settings

493 (Gao et al., 2004), and will form a large number of Mg-rich (Mg#>50) rocks due to the

494 partial melting of lithospheric mantle and/or upwelling of asthenosphere (Ou et al.,

495 2017). However, these Jurassic magmatic rocks in the Liaodong Peninsula are generally

considered to be formed in a compressional environment related to the subduction of the Paleo-Pacific slab (Li et al., 2004; Yang et al., 2015a; Zhu and Xu, 2019; Zheng et al., 2018). Furthermore, the middle-late Jurassic granites are generally Mg-poor (Fig. 13c).Due to the high temperature of the asthenosphere (1200 °C, Parsons and McKenzie, 1978; King et al., 2015), rocks formed by partial melting of the delaminated lower crust should possess a high-temperature fingerprint. T_{Zrn} has been used as a geothermometer to estimate partial melting temperatures (e.g., Miller et al., 2003; Collins et al., 2016). As mentioned before, the T_{Zrn} of the Zhoujiapuzi granite is below 900 °C, which is markedly lower than the temperature of the asthenosphere. Therefore, the petrogenetic model of delaminated lower continental crust (Model B) is also inconsistent with the Zhoujiapuzi granite.

6.3.3 Model C: Differentiation of basaltic arc magma

Low-pressure fractional crystallization (involving olivine + clinopyroxene + plagioclase + amphibole+ titanomagnetite) or high-pressure fractional crystallization (involving garnet) from basaltic magmas have been proposed as two ways to generate adakitic characteristics (Castillo et al., 1999; Macpherson et al., 2006).

However, the composition of the Zhoujiapuzi granite is relatively uniform, including SiO_2, MgO and Na_2O, which does not support major fractional crystallization (Xue et a., 2017). Furthermore, the Zhoujiapuzi granite has abundant inherited zircons and no obvious depletion of Sr, Eu and Ba, showing that this granite has not experienced extensive fractionation (Miller et al., 2003). The samples form clear partial melting trends on the La/Yb versus La diagram (Fig. 13e), which also suggests that partial melting was more important than fractional crystallization (Gao et al., 2007; Shahbazi et al., 2021). In addition, crystal fractionation of basaltic melts can only form minor

volumes of granitic melts, the ratio of the two is about 9:1 (Zeng et al., 2016). However, for the same age interval, no coexisting mafic-intermediate rocks have been found in the research area. In the wider region of the Liaodong Peninsula, Middle-Late Jurassic magmatism is dominated by felsic compositions; mafic- intermediate rocks are only reported in the Huaziyu area (lamprophyre dikes, Jiang et al., 2005). Therefore, it is unlikely that there are large-scale mafic- intermediate rocks contemporaneous with the Zhoujiapuzi granite at depth according to the rock assemblage of Liaodong Peninsula in this period. Moreover, the zircon Hf isotopic compositions of the Zhoujiapuzi granite are quite different from those of the depleted mantle, but are similar to those of the basement (Liaohe Group and Liaoji granite) in the study area (Fig. 8). The ancient inherited zircons (2500 to 2173) with low εHf(t) values also indicate older crustal material in the Zhoujiapuzi granite. For these reasons, it is highly improbable that Zhoujiapuzi granite was derived by differentiation of basaltic magma (Model C).

6.3.4 Model D: Magma mixing between mantle-derived mafic and crust-derived silicic magmas

The Zhoujiapuzi granite has high K_2O/Na_2O ratio (>1) and A/CNK value (>1), together with the absence of mingling textures, mafic microgranular enclaves (MMEs), felsic xenocrysts and melting texture of plagioclase, implying that the mantle-derived magma is unlikely to have played an important role in the genesis of the Zhoujiapuzi granite (Castro et al., 1991). In addition, the Zhoujiapuzi granite is characterized by the development of biotite, but lacks amphibole and pyroxene. These features, coupled with the high A/CNK value, are consistent with an origin as a crust-derived granitoid, but obviously different from the granitoids formed by crust-mantle-derived magma mixing (Barbarin, 1990). Moreover, granites formed by magma mixing generally have high

544 MgO, TFe$_2$O$_3$, CaO and Cr contents and low SiO$_2$ content (Ma et al., 2013a; Wang et

545 al., 2018). These features are obviously inconsistent with the Zhoujiapuzi granite in this

546 study. Additionally, the εHf(t) values and trace element composition of the two stages

547 of zircon also do not support magma mixing. Hence, magma mixing of mantle-derived

548 and crust-derived magmas (Model D) is also unlikely to have produced the Zhoujiapuzi

549 granite.

6.3.5 Model E: Partial melting of thickened basaltic LCC

551   Experimental studies have shown that the partial melt of basaltic LCC in the garnet

552 stabilization zone (> 40 km, i.e. ~1.2 GPa) can produce magma with a high Sr/Y ratio

553 (Rapp et al., 2003 and references therein). In these scenarios, high Sr/Y and overall

554 adakitic affinity are caused by leaving garnet as residual phases (e.g. Gao et al., 2004).

555 Based on geochemical data for the Zhoujiapuzi granites, partial melting of thickened

556 basaltic LCC is also unlikely to account for the high Sr/Y Zhoujiapuzi granite (Model

557 E). This conclusion is based on the following observations:

558   (1) This ratio of (Gd/Yb)$_N$ is the most important feature to judge whether garnet is

559 involvement in magma genesis (Ma et al., 2012). If the (Gd/Yb)$_N$ ratio of the source is

560 similar to the average value of the LCC (1.71, Rudnick and Gao, 2003), partial melting

561 of these crustal materials controlled by garnet at high pressure can produce melt with

562 (Gd/Yb)$_N$ of 5.8 (Huang and He, 2010). In contrast, the (Gd/Yb)$_N$ values (1.22–5.06,

563 average 2.69) of the Zhoujiapuzi granite are relatively low. (2) Studies of lower-crustal

564 xenoliths show that garnet may not be a common mineral in the lower crust of the NCC

565 (Ma et al., 2012). (3) As shown in the discrimination diagrams of granite sources (Fig.

566 13f, g), all samples fall in the range of metagreywacke-derived melts. Therefore, the

567 Zhoujiapuzi granite was considered to have been derived from crustal anatexis of

metagraywacke (or intermediate-acid igneous rock with similar mineral composition), rather than basaltic lower crust.

6.3.6 Model F: Melting of a high Sr/Y (and La/Yb) source

Studies have shown that when a source rock has a high Sr/Y ratio, the high Sr/Y signature of the derived magma can inherit from their source, regardless of pressure (Kamei et al., 2009; Moyen, 2009; Ma et al., 2015). We suggest that partial melting of high Sr/Y Liaoji granite was most probably the origin of the high Sr/Y Zhoujiapuzi granite, as discussed below (Model F).

The Zhoujiapuzi granite has similar mineral assemblages (contains abundant K-feldspar and lacks hornblende) and geochemical composition (Fig. 13h) to the Tsutsugatake intrusion, which is explained by partial melting of arc-type tonalite or adakitic granodiorite (Kamei et al., 2009). Among the inherited zircons from Zhoujiapuzi granite, the ^{207}Pb / ^{206}Pb ages of all the spots are between 2132 and 2200 Ma, except one, and yield a Concordia upper intercept age of 2163 Ma. Both assimilation of country-rocks and incomplete melting of source rocks can explain the genesis of inherited zircon in granite. Due to the similar T_{DM2} of autocrystic zircons (light-CL core and dark-CL rim) and inherited zircons, these inherited zircons most likely come from the source of the Zhoujiapuzi granite. In the study area, meta-sedimentary rocks and meta-volcanic rocks of the South Liaohe Group, Paleoproterozoic mafic rocks, as well as the Liaoji granites, have ~2.16 Ga zircon. In spite of an age peak of 2.17–2.16 Ga in detrital zircon age spectra of the metasediments from the South Liaohe Group, melting of a sediment-dominated source is unlikely to have occurred, as it would have also introduced other age peaks such as ~2.03 Ga and ~2.50 Ga (Li et al., 2015; Wang et al., 2020b). In addition, given the I-type

592   characteristics of the Zhoujipuzi granite, derivation from an igneous precursor is more

593   plausible rather than a metasedimentary origin (Chappell and White, 1992). Therefore,

594   these ~2.16 Ga zircons from the Zhoujiapuzi granite are unlikely to come from the

595   South Liaohe Group. As shown in the host rock discrimination diagrams (Fig. 14,

596   introduced by Belousova et al., 2002), all the ~2.16 Ga inherited zircons from

597   Zhoujiapuzi granite fall into the granitoid area (Fig. 14), precluding that these ~2.16 Ga

598   zircon come from the Paleoproterozoic mafic rocks. In addition, the ~2.16 Ga inherited

599   zircons from Zhoujiapuzi granite and the zircons from the Liaoji granites lie in a similar

600   area in the εHf(t)-age (Ma) diagram (Fig. 8). Hence, the ~2.16 Ga inherited zircon most

601   likely come from the Liaoji granites.

602   Some of the Liaoji granites, such as the Muniuhe granite (comprising granodiorite

603   and syenogranite with no distinct boundary between the two), have adakitic signatures,

604   and similar REE and trace element patterns as the Zhoujiapuzi granite (Fig. 4). Based

605   on a model of batch melting (Shaw, 1970) using the experiments of Conrad et al. (1988),

606   the high Sr/Y characteristic of the Zhoujiapuzi granite can be explained by partial

607   melting of Muniuhe granitic pluton leaving amphibole as the main residue (Fig. 12b).

608   In our modelling, we choose the XY-005 sample to approximately represent the

609   primitive melt composition. The reasons are as below: as mentioned above, the high

610   Sr/Y characteristics of the Zhoujiapuzi granite are not caused by the fractional

611   crystallization of amphibole. Furthermore, the lack of positive correlation between

612   Dy_N/Yb_N ratios and La_N/Yb_N ratios (Fig. 13i) also suggests that fractional

613   crystallization of amphibole was not a significant process for the Zhoujiapuzi granite.

614   On the other hand, the samples of Zhoujiapuzi granite display variable Eu and Sr

615   contents, implying that plagioclase is likely a fractional phase. The separation of

616   titanomagnetite could explain the positive trend in TFe_2O_3 with increasing TiO_2 content,

consistent with the occurrences of magnetite in some studied rocks. This possible mineral assemblage of fractional crystallization is also reflected by the chemical variations in the Sr/Y-Y diagram (Fig. 12b). Hence, the sample XY-005, which has highest Sr/Y, was chosen to represent a primitive melt composition. To find the best matching experimental melts, we have compared the major elements of the XY-005 sample with that of experimental melts and the characteristics of no garnet residue discussed above. Results are shown in Fig. 12b. The Sr and Y compositions of the starting material used in these experiments resemble those of the average composition of the Muniuhe granitic pluton (Sr=475 ppm, Y=9.77 ppm), if the residue contains a large volume of amphibole (>90 %). However, if more plagioclase is retained in the residue (e.g. 18.3 %), a source region with a higher Sr content is required. Therefore, a similar high Sr/Y Liaoji granite to the Muniuhe granitic pluton can produce the high Sr/Y signatures of the Zhoujiapuzi granite.

A large number of Yanshanian adakites (or high Sr/Y rocks) are developed in the NCC, which are generally considered to be derived from the thickened basaltic LCC (e.g. Gao et al., 2004; Wu et al., 2005a; Ma et al., 2013b). Zhang et al. (2001, 2003) suggested that these so-called "C-type adakites" indicated a large-scale crustal thickening event. However, according to the studies on the Triassic and Jurassic adakitic rocks near the Pingquan area, the northern part of the NCC, Ma et al. (2012, 2015) suggested that the adakitic signatures of these rocks are inherited from their source rocks. The research of the Zhoujiapuzi granite in this study also shows that among the widely distributed Jurassic high Sr/Y granites in the Liaodong Peninsula, there is at least one pluton with a high Sr/Y signature inherited from the source. Therefore, we suggest that melting of a high Sr/Y (and La/Yb) source is one of the important processes for the generation of Yanshanian high Sr/Y rocks in the NCC. This kind of high Sr/Y

642 granite does not need to be formed in the garnet stability field.

643 **6.4 Tectonic implications**

644   A large number of Early Jurassic arc-like igneous rocks occur in the northeast part

645 of NCC- Korean Peninsula-Hida belt, which belong to the middle-high K calc-alkaline

646 series and are characterized by enrichment in LILE and depletions in HFSE (Wu et al.,

647 2007; Tang et al., 2018 and references therein). In addition, the Early Jurassic

648 accretionary complexes in the eastern margin of the Eurasian continent and the Japan

649 islands, such as the Heilongjiang complex, the Khabarovsk complex and the Mino-

650 Tamba complex, are considered to be related to subduction (Wu et al., 2007; Tang et al.,

651 2018 and references therein). It is generally accepted that the Paleo-Pacific slab

652 subducted westwards in the Early Jurassic (Tang et al., 2018; Zhu and Xu, 2018).

653   In the middle-late Jurassic, I-type granites are dominant in the Liaodong Peninsula,

654 such as the Zhoujiapuzi granite (this study), Heigou pluton, Gaoliduntai pluton (Wu et

655 al., 2005a), Waling granite (Yang et al., 2015a) and Wulong granite (Yang et al., 2018).

656 There are not A-type granites, and mantle derived magmatism is extremely rare. These

657 granites were formed by partial melting of crustal materials without obvious

658 contribution of mantle derived magma (Wu et al., 2005a; Yang et al., 2015b, 2018; Xue

659 et al., 2020). In addition, WNW-ESE compression during 157-143 Ma was widespread

660 in the Liaodong Peninsula (Yang et al., 2004; Zhang et al., 2020). It not only

661 mylonitized the granite plutons in middle-lower crust levels, but also intensely

662 deformed the thick sedimentary cover in the upper crust (Qiu et al., 2018; Ren et al.,

2020). Hence, Late Jurassic magmatism in the Liaodong peninsula is most likely to be related to subduction of the Paleo-Pacific plate in a mature continental arc, with crust previously thickened by compressional tectonics, related to both the oceanic subduction and the earlier Mesozoic collisions at the north and south margins of the NCC. This setting would produce the conditions required for extensive crustal melting of pre-existing basement. There is a potential resemblance to the modern arc of the Central Andes (Allmendinger et al., 1997), where crustal thickening and plateau growth has developed over the Cenozoic (Scott et al., 2018), and melting of older basement has taken place during subduction of the Nazca plate (Miller and Harris, 1989). This model is also consistent with the idea that much of eastern China was a high orogenic plateau during the Mesozoic, before widespread Early Cretaceous extension and core complex development (Meng, 2003; Chu et al., 2020).

7. Conclusions

(1) LA-ICP-MS zircon U-Pb dating indicates that the Zhoujiapuzi granite in the Liaodong Peninsula formed at ~160 Ma.

(2) Zircon growth in Zhoujiapuzi granite can be divided into two distinct stages. The light-CL core was formed in a deeper, hotter, magma chamber, which had low oxygen fugacity and high temperature. The dark-CL rim formed from later, more evolved, magma. Oxygen fugacity significantly increased and the temperature

decreased at this stage. The Zhoujiapuzi granite is a case study of multistage generation and emplacement of magma, revealed by zircons, where no signals are discernible in the bulk petrology or geochemistry.

(3) The I-type Zhoujiapuzi granite originated from partial melting of the Paleoproterozoic Liaoji granites. The high Sr/Y compositions are inherited from their source rocks, rather than being a direct indication of deep crustal melting, or any other common mechanism for generating adakitic signatures.

(4) The Late Jurassic tectonic setting of the Liaodong Peninsula and the eastern NCC resembled the modern orogenic plateau of the Central Andes, where silicic magmatism may occur by partial melting of older continental crust in a compressional environment, related to the subduction of the Paleo-Pacific plate.

Acknowledgements

We thank Dr. Wenzhou Xiao, Dr. Jiajie Chen and Dr. Quan Ou for constructive reviews and useful suggestions. We are also grateful to Ying Liu, Chunying Guo, Jianxiong Hu, Ziming Hu for their help with the field work. This research was funded by the National Nature Science Foundation of China (Grants No. 42030809, 41772349, 41902075, 42002095; 42162013), China Scholarship Council (No. 202008360018), Geological Exploration Program of China Nuclear Geology (Grant No. D1802), the research grants from the East China University of Technology (Grant No. DHBK2017103), Open Research Fund Program of State Key Laboratory of Nuclear Resources and Environment (East China University of Technology) (Grant 2020NRE13).

References

706   Allmendinger, R. W., Jordan, T. E., Kay, S. M., and Isacks, B. L.: The evolution of the

707   Altiplano-Puna plateau of the Central Andes, Annu. Rev. Earth Pl. Sc., 25, 139–

708   174, https://doi.org/10.1146/annurev.earth.25.1.139, 1997.

709   Altherr, R., Holl, A., Hegner, E., Langer, C. and Kreuzer, H.: High-potassium, calc-

710   alkaline I-type plutonism in the European Variscides: northern Vosges (France)

711   and   northern   Schwarzwald   (Germany),   Lithos,   50(1-3),   51–73,

712   https://doi.org/10.1016/S0024-4937(99)00052-3, 2000.

713   Ballard, J. R., Palin, M. J., and Campbell, I. H.: Relative oxidation states of magmas

714   inferred from Ce(IV)/Ce(III) in zircon: application to porphyry copper deposits of

715   northern   Chile.   Contrib.   Mineral.   Petrol.,   144,   347–364,

716   https://doi.org/10.1007/s00410-002-0402-5, 2002.

717   Barbarin, B.: Granitoids: main petrogenetic classifification in relation to origin and

718   tectonic setting, Geol. J., 25, 227–238, 1990.

719   Belousova, E., Griffin, W., O'Reilly, S. Y., and Fisher, N.: Igneous zircon: trace

720   element composition as an indicator of source rock type, Contrib. Mineral. Petrol.,

721   143, 602–622, https://doi.org/10.1007/s00410-002-0364-7, 2002.

722   Blichert-Toft, J., and Albarède, F.: The Lu-Hf isotope geochemistry of chondrites and

723   the evolution of the mantle-crust system, Earth. Planet. Sc. Lett., 148(1), 243–258,

724   https://doi.org/10.1016/S0012-821X(97)00040-X, 1997.

725   Breiter, K., Lamarão, C. N., Borges, R. M. K., and Dall'Agnol, R.: Chemical

726   characteristics of zircon from A-type granites and comparison to zircon of S-type

727   granites, Lithos, 192–195, 208–225, https://doi.org/10.1016/j.lithos.2014.02.004,

728   2014.

729   Castillo, P. R., Janney, P. E., and Solidum, R. U.: Petrology and geochemistry of

730   Camiguin Island, southern Philippines: Insights to the source of adakites and other

731   lavas in a complex arc setting, Contrib. Mineral. Petrol., 134(1), 33–51,

732   https://doi.org/10.1007/s004100050467, 1999.

733   Castro, A., Moreno-Ventas, I., and Rosa, J.: H-type (hybrid) granitoids: a proposed

734   revision of the granite-type classification and nomenclature, Earth. Sci. Rev., 31,

735   237–253, https://doi.org/10.1016/0012-8252(91)90020-G, 1991.

736   Chappell, B. W., and White, A. J. R.: I-and S-type granites in the Lachlan Fold Belt,

737   Geol. Soc. Am. Spec. Pap., 272, 1–26, https://doi.org/10.1130/SPE272-p1, 1992.

738   Chen, S. R., Wang, Q., Zhu, D. C., Weinberg, R. F., Zhang, L. L., and Zhao, Z. D.:

739   Reheating and magma mixing recorded by zircon and quartz from high-silica

740   rhyolite in the Coqen region, southern Tibet, Am. Miner.,

741   https://doi.org/10.2138/am-2020-7426, 2020.

742   Chu, Y., Lin, W., Faure, M., Allen, M. B., and Feng, Z.: Cretaceous exhumation of the

743   Triassic intracontinental Xuefengshan Belt: Delayed unroofing of an orogenic

744   plateau across the South China Block? Tectonophysics, 793, 228592,

745   https://doi.org/1016/j.tecto.2020.228592, 2020.

746   Claiborne, L. L., Miller, C. F., Walker, B. A., Wooden, J. L., Mazdab, F. K., and Bea,

747   F.: Tracking magmatic processes through Zr/Hf ratios in rocks and Hf and Ti

748   zoning in zircons: An example from the Spirit Mountain batholith, Nevada.

749   Mineral. Mag., 70, 517–543, https://doi.org/10.1180/0026461067050348, 2006.

Collins, W. J., Beams, S. D., White, A. J. R., and Chappell, B. W.: Nature and origin of A-type granites with particular reference to southeastern Australia, Contrib. Mineral. Petr., 80, 189-200, https://doi.org/10.1007/BF00374895, 1982.

Collins, W. J., Huang, H. Q., and Jiang, X. Y.: Water-fluxed crustal melting produces Cordilleran batholiths, Geology, 44(2), 143–146, https://doi.org/10.1130/G37398.1, 2016.

Conrad, W. K., Nicholls, I. A., and Wall, V. J.: Water-saturated and -undersaturated melting of metaluminous and peraluminous crustal compositions at 10 kb: evidence for the origin of silisic magmas in the Taupo Volcanic Zone, New Zealand, and other occurrences, J. Petrol., 29, 765–803, https://doi.org/10.1093/petrology/29.4.765, 1988.

Defant, M. J., and Drummond, M. S.: Derivation of some modern arc magmas by melting of young subducted lithosphere, Nature, 347, 662–665, https://doi.org/10.1038/347662a0, 1990.

Douce, A. E. P.: Generation of metaluminous A-type granites by low-pressure melting of calc-alkaline granitoids, Geology, 25, 743–746, https://doi.org/10.1130/0091-7613(1997)025<0743:GOMATG>2.3.CO;2, 1997.

Drummond, M. S., Defant, M. J., and Kepezhinskas, P. K.: Petrogenesis of slab-derived trondhjemite–tonalite–dacite/adakite magmas, Trans. R. Soc. Edinb., 87, 205–215, https://doi.org/10.1017/S0263593300006611, 1996.

Faure, M., Lin, W., Moni, P., and Bruguier, O.: Paleoproterozoic arc magmatism and collision in Liaodong Peninsula, NE China, Terra. Nova., 16, 75–80,

https://doi.org/10.1111/j.1365-3121.2004.00533.x, 2004.

Ferry, J. M., and Watson, E. B.: New thermodynamic models and revised calibrations for the Ti-in-zircon and Zr-in-rutile thermometers, Contrib. Mineral. Petrol., 154, 429–437, https://doi.org/10.1007/s00410-007-0201-0, 2007.

Frost, B. R., Barnes, C. G., Collins, W. J., Arculus, R. J., Ellis, D. J., and Frost, C. D.: A geochemical classification for granitic rocks, J. Petrol., 42, 2033–2048, https://doi.org/10.1093/petrology/42.11.2033, 2001.

Gao, S., Rudnick, R. L., Yuan, H. L., Liu, X. M., Liu, Y. S., Xu, W. L., Ling, W. L., Ayers, J. C., Wang, X. C., and Wang, Q. H.: Recycling lower continental crust in the North China craton, Nature, 432, 892–897, https://doi.org/10.1038/nature03162, 2004.

Gao, Y. F., Hou, Z. Q., Kamber, B. S., Wei, R. H., Meng, X.J., and Zhao, R. S.: Adakite-like porphyries from the southern Tibetan continental collision zones: evidence for slab melt metasomatism, Contrib. Mineral. Petr., 153, 105–20, 10.1007/s00410-006-0137-9, 2007.

Griffin, W. L., Belousova, E. A., Shee, S. R., Pearson, N. J., and O'Reilly, S. Y.: Archean crustal evolution in the northern Yilgarn Craton: U-Pb and Hf-isotope evidence from detrital zircons, Precambrian. Res., 131, 231–282, https://doi.org/10.1016/J.PRECAMRES.2003.12.011, 2004.

He, P. L., Huang, X. L., Yang, F., and Wang, X.: Mineralogy constraints on magmatic processes controlling adakitic features of Early Permian high-magnesium diorites in the Western Tianshan orogenic belt, J. Petrol., 61, a114,

794   https://doi.org/10.1093/petrology/egaa114, 2021.

795   Hoskin, P. W. O.: Trace-element composition of hydrothermal zircon and the alteration

796   of Hadean zircon from the Jack Hills, Australia, Geochim. Cosmochim. Ac., 69,

797   637–648, https://doi.org/10.1016/j.gca.2004.07.006, 2005.

798   Hoskin, P. W., and Schaltegger, U.: The composition of zircon and igneous and

799   metamorphic   petrogenesis,   Rev.   Mineral.   Geochem.,   53,   27–62,

800   https://doi.org/10.2113/0530027, 2003.

801   Huang, F., and He, Y.S.: Partial melting of the dry mafic continental crust: Implications

802   for petrogenesis of C-type adakites, Chinese. Sci. Bull., 55, 1255–1267,

803   https://doi.org/10.1007/s11434-010-3224-2, 2010.

804   Jackson, S. E., Pearson, N. J., Griffin W L, and Belousova, E. A.: The application of

805   laser ablation-inductively coupled plasma-mass spectrometry to in situ U-Pb

806   zircon   geochronology,   Chem.   Geol.,   211(1-2),   47–69,

807   https://doi.org/doi:10.1016/j.chemgeo.2004.06.017, 2004.

808   Jiang, H., Jiang, S. Y., Li, W. Q., Zhao, K. D., and Peng, N. J.: Highly fractionated

809   Jurassic I-type granites and related tungsten mineralization in the Shirenzhang

810   deposit, northern Guangdong, South China: Evidence from cassiterite and zircon

811   U-Pb ages, geochemistry and Sr-Nd-Pb-Hf isotopes, Lithos, S480187509,

812   https://doi.org/10.1016/j.lithos.2018.04.030, 2018.

813   Jiang, Y.H., Jiang, S.Y., Zhao, K.D., Ni, P., Ling, H.F., and Liu, D.Y.: SHRIMP U-Pb

814   zircon dating for lamprophyre from Liaodong Peninsula: Constraints on the initial

815   time of Mesozoic lithosphere thinning beneath eastern China, Chinese. Sci. Bull.,

816   50, https://doi.org/10.1360/982005-373, 2612–2620, 2005.

817   Kamei, A., Miyake, Y., Owada, M., and Kimura, J.: A pseudo adakite derived from

818   partial melting of tonalitic to granodioritic crust, Kyushu, southwest Japan arc,

819   Lithos, 112, 615–625, https://doi.org/10.1016/j.lithos.2009.05.024, 2009.

820   Kay, R. W., and Kay, S. M.: Delamination and delamination magmatism,

821   Tectonophysics, 219, 177–189, https://doi.org/10.1016/0040-1951(93)90295-U,

822   1993.

823   King, S. D., Frost, D. J., and Rubie D. C.: Why cold slabs stagnate in the transition zone,

824   Geology, 43(3), 231–234, https://doi.org/10.1130/G36320.1, 2015.

825   Li, C.M., Zhang, C.H., Cope, T.D., and Lin, Y.: Out-of-sequence thrusting in polycyclic

826   thrust belts: An example from the Mesozoic Yanshan belt, North China Craton,

827   Tectonics, 35, 2082–2116, https://doi.org/10.1002/2016TC004187, 2016.

828   Li, S. Z., and Zhao, G. C.: SHRIMP U-Pb zircon geochronology of the Liaoji granitoids:

829   Constraints on the evolution of the Paleoproterozoic Jiao-Liao-Ji belt in the

830   Eastern Block of the North China Craton, Precambrian. Res., 158, 1–16,

831   https://doi.org/10.1016/j.precamres.2007.04.001, 2007.

832   Li, S. Z., Zhao, G. C., Sun, M., Han, Z. Z., Hao, D. F., Luo, Y., and Xia, X. P.:

833   Deformation history of the Paleoproterozoic Liaohe Group in the Eastern Block

834   of the North China Craton, J. Asian. Earth. Sci., 24, 659–674, https://doi.org/659–

835   67410.1016/j.jseaes.2003.11.008, 2005.

836   Li, S.Z., Liu, J.Z., Zhao, G.C., Wu, F.Y., Han, Z.Z., and Yang, Z.Z.: Key

837   geochronology of Mesozoic deformation in the eastern block of the North China

838   Craton and its constraints on regional tectonics: A case of Jiaodong and Liaodong

839   Peninsula, Acta. Petrol. Sin., 2, 633–646, https://doi.org/10.1007/BF02873097,

840   2004.

841   Li, X.H., Long, W.G., Li, Q.L., Liu, Y., Zheng, Y.F., Yang, Y.H., Chamberlain, K.R.,

842   Wan, D.F., Guo, C.H., and Wang, X.C.: Penglai Zircon Megacrysts: A Potential

843   New Working Reference Material for Microbeam Determination of Hf-O Isotopes

844   and   U-Pb   Age,   Geostand.   Geoanal.   Res.,   34,   117–134,

845   https://doi.org/info:doi/10.1111/j.1751-908X.2010.00036.x, 2010.

846   Li, Z., Chen, B., Liu, J.W., Zhang, L., and Yang, C.: Zircon U-Pb ages and their

847   implications for the South Liaohe Group in the Liaodong Peninsula, Northeast

848   China (in Chinese with English abstract), Acta. Petrol. Sin., 31(6), 1589–1605,

849   2015.

850   Liu, Y.S., Hu, Z.C., Zong, K.Q., Gao, C.G., Gao, S., Xu, J., and Chen, H.H.:

851   Reappraisement and refinement of zircon U-Pb isotope and trace element analyses

852   by   LA-ICP-MS,   Chinese.   Sci.   Bull.,   55,   1535–1546,

853   https://doi.org/10.1007/s11434-010-3052-4, 2010.

854   Loader, M. A., Wilkinson, J. J., and Armstrong, R. N.: The effect of titanite

855   crystallisation on Eu and Ce anomalies in zircon and its implications for the

856   assessment of porphyry Cu deposit fertility, Earth. Planet. Sc. Lett., 472, 107–119,

857   https://doi.org/10.1016/j.epsl.2017.05.010, 2017.

858   Ludwig, K. R.: User's manual for Isoplot 3.00: a geochronological toolkit for Microsoft

859   Excel, Berkeley. Geochronology. Center., 2003.

Ma, L., Jiang, S.Y., Dai, B.Z., Jiang, Y.H., Hou, M.L., Pu, W., and Xu, B.: Multiple sources for the origin of Late Jurassic Linglong adakitic granite in the Shandong Peninsula, eastern China: Zircon U-Pb geochronological, geochemical and Sr-Nd-Hf isotopic evidence, Lithos, 162–163, 251–263, https://doi.org/10.1016/j.lithos.2013.01.009, 2013b.

Ma, Q., Zheng, J.P., Griffin, W. L., Zhang, M., Tang, H.Y., Su, Y.P., and Ping, X.Q.: Triassic "adakitic" rocks in an extensional setting (North China): Melts from the cratonic lower crust, Lithos, 149, 159–173, https://doi.org/10.1016/j.lithos.2012.04.017, 2012.

Ma, Q., Zheng, J.P., Xu, Y.G., Griffin, W. L., and Zhang, R.S.: Are continental "adakites" derived from thickened or foundered lower crust? Earth. Planet. Sc. Lett., 419, 125–133, https://doi.org/10.1016/j.epsl.2015.02.036, 2015.

Ma, X.H., Chen, B., and Yang, M.C.: Magma mixing origin for the Aolunhua porphyry related to Mo-Cu mineralization, eastern Central Asian Orogenic Belt, Gondwana. Res., 24, 1152–1171, https://doi.org/10.1016/j.gr.2013.02.010, 2013a.

Macpherson, C. G., Dreher, S. T., and Thirlwall, M. F.: Adakites without slab melting: High pressure differentiation of island arc magma, Mindanao, the Philippines, Earth. Planet. Sc. Lett., 243(3), 581–593, https://doi.org/10.1016/j.epsl.2005.12.034, 2006.

Mahon, K. I.: The New "York" regression: Application of an improved statistical method to geochemistry, Int. Geol. Rev., 38(4), 293–303, https://doi.org/10.1080/00206819709465336, 1996.

882 Maniar, P. D., and Piccoli, P. M.: Tectonic discrimination of granitoids, Geol. Soc. Am.

883 Bull., 101, 635–643, https://doi.org/10.1130/0016-

884 7606(1989)101<0635:TDOG>2.3.CO;2, 1989.

885 Martin, H., Smithies, R.H., Rapp, R., Moyen, J.-F., and Champion, D.: An overview of

886 adakite, tonalite-trondhjemite-granodiorite (TTG), and sanukitoid: relationships

887 and some implications for crustal evolution, Lithos, 79, 1–24,

888 https://doi.org/10.1016/j.lithos.2004.04.048, 2005.

889 Meng, E., Liu, F.L., Liu, P.H., Liu, C.H., Yang, H., Wang, F., Shi, J.R., and Cai, J.:

890 Petrogenesis and tectonic significance of Paleoproterozoic meta-mafic rocks from

891 central Liaodong Peninsula, northeast China: Evidence from zircon U-Pb dating

892 and in situ Lu-Hf isotopes, and whole-rock geochemistry, Precambrian. Res., 247,

893 92–109, https://doi.org/10.1016/j.precamres.2014.03.017, 2014.

894 Meng, Q. R.: What drove late Mesozoic extension of the northern China-Mongolia tract?

895 Tectonophysics, 369, 155–174, https://doi.org/0.1016/S0040-1951(03)00195-1,

896 2003.

897 Mezger, K., and Krogstad, E. J.: Interpretation of discordant U-Pb zircon ages: An

898 evaluation, J. Metamorph. Geol., 15, 127–140, https://doi.org/10.1111/j.1525-

899 1314.1997.00008.x,1997.

900 Miller, C. F., McDowell, S. M., and Mapes, R. W.: Hot and cold granites? Implications

901 of zircon saturation temperatures and preservation of inheritance, Geology, 31,

902 529–532, https://doi.org/10.1130/0091-7613(2003)031<0529:hacgio>2.0.co;2,

903 2003.

Miller, J.F., and Harris, N.B.W.: Evolution of continental crust in the Central Andes; constraints from Nd isotope systematics, Geology, 17, 615–617, https://doi.org/10.1130/0091-7613(1989)0172.3.CO;2, 1989.

Moyen, J.: High Sr/Y and La/Yb ratios: The meaning of the "adakitic signature", Lithos, 112, 556–574, https://doi.org/10.1016/j.lithos.2009.04.001, 2009.

Nakamura, H., and Iwamori, H.: Generation of adakites in a cold subduction zone due to double subducting plates, Contrib. Mineral. Petr., 165, 1107–1134, https://doi.org/10.1007/s00410-013-0850-0, 2013.

Nasdala, L., Pidgeon, R. T., Wolf, D., and Irmer, G., Metamictization and U-Pb isotopic discordance in single zircons: a combined Raman microprobe and SHRIMP ion probe study, Miner. Petrol., 62, 1–27, https://doi.org/10.1007/BF01173760, 1998.

Nash, D.J., Ciborowski, T., Ullyott, J.S., Pearson, M.P. and Whitaker, K.A.: Origins of the sarsen megaliths at Stonehenge, Sci. Adv., 6, eabc0133, https://doi.org/10.1126/sciadv.abc0133, 2020.

Ou, Q., Wang, Q., Wyman, D. A., Zhang, H.X., Yang, J.H., Zeng, J.P., Hao, L.L., Chen, Y.W., Liang, and H., Qi, Y.: Eocene adakitic porphyries in the central-northern Qiangtang Block, central Tibet: Partial melting of thickened lower crust and implications for initial surface uplifting of the plateau, J. Geophys. Res. Solid. Earth., 122, 1025–1053, https://doi.org/10.1002/2016JB013259, 2017.

Parsons, B., and Dan, M.K.: Mantle convection and the thermal structure of the plates, J. Geophys. Res. Solid. Earth., 83, https://doi.org/10.1029/JB083iB09p04485, 1978.

Patiño Douce, A.E.P.: What do experiments tell us about the relative contributions of crust and mantle to the origin of granitic magmas? Geol. Soc. Lond. Spec. Publ., 168(1), 55–75, https://doi.org/10.1144/GSL.SP.1999.168.01.05, 1999.

Qiu, L., Kong, R.Y., Yan, D.P., Wells, M.L., Wang, A.P., Sun, W.H., Yang, W.X., Han, Y.G., Li, C.M., and Zhang, Y.X.: The Zhayao tectonic window of the Jurassic Yuantai thrust system in Liaodong Peninsula, NE China: Geometry, kinematics and tectonic implications, J. Asian Earth Sci., 164, 58–71, https://doi.org/10.1016/j.jseaes.2018.06.012, 2018.

Rapp, R. P., Shimizu, N and Norman, M.D.: Growth of early continental crust by partial melting of eclogite, Nature, 425(6958), 605–609, https://doi.org/10.1038/nature02031, 2003.

Ren, Z.H., Lin, W., Faure, M., Meng, L.T., Qiu, H.B., and Zeng, J.P.: Triassic- Jurassic evolution of the eastern North China Craton: Insights from the Lushun-Dalian area, South Liaodong Peninsula, NE China, Geol. Soc. Am. Bull., 133(1–2), https://doi.org/10.1130/B35533.1, 2020.

Rudnick, R. L., and Gao, S.: Composition of the continental crust, Treatise. Geochem., 3, 1–64, https://doi.org/10.1016/b0-08-043751-6/03016-4, 2003.

Schiller, D., and Finger, F.: Application of Ti-in-zircon thermometry to granite studies: problems and possible solutions, Contrib. Mineral. Petr., 174, https://doi.org/10.1007/s00410-019-1585-3, 2019.

Schmitz, M. D., and Kuiper, K. F.: High-Precision Geochronology, Elements., 9, 25–30, https://doi.org/10.2113/gselements.9.1.25, 2013.

Schwartz, J. J., Johnson, K., Miranda, E. A., and Wooden, J. L.: The generation of high Sr/Y plutons following Late Jurassic arc–arc collision, Blue Mountains province, NE Oregon, Lithos, 126, 22–41, https://doi.org/10.1016/j.lithos.2011.05.005, 2011.

Scott, E.M., Allen, M.B., Macpherson, C.G., McCaffrey, K.J.W., Davidson, J.P., Saville, C., and Ducea, M.N.: Andean surface uplift constrained by radiogenic isotopes of arc lavas, Nat. Commun., 9(1), 969, https://doi.org/10.1038/s41467-018-03173-4, 2018.

Shahbazi, H., Maghami, Y. T., Azizi, H., Asahara, Y., Siebel, Y., Maanijou, M., and Rezai, A.: Zircon U-Pb ages and petrogenesis of late Miocene adakitic rocks from the Sari Gunay gold deposit, NW Iran, Geol. Mag., https://doi.org/10.1017/S0016756821000297, 2021.

Shannon. R.D.: Revised effective ionic radii and systematic studies of interatomic distances in halides and chalcogenides, Acta. Crystall. A., 32(5), 751–767, https://doi.org/10.1107/S0567739476001551, 1976.

Shaw, D.M.: Trace element fractionation during anatexis, Geochim. Cosmochim. Ac., 34, 237–243, https://doi.org/10.1016/0016-7037(70)90009-8, 1970.

Siégel, C., Bryan, S. E., Allen, C. M., and Gust, D. A.: Use and abuse of zircon-based thermometers: A critical review and a recommended approach to identify antecrystic zircons, Earth. Sci. Rev., 176, 87–116, https://doi.org/10.1016/j.earscirev.2017.08.011, 2018.

Skjerlie, K. P., and Johnston, A. D.: Vapor-absent melting at 10 kbar of a biotite-and

amphibole-bearing tonalitic gneiss: implications for the generation of A-type granites, Geology, 20, 263–266, https://doi.org/10.1130/0091-7613(1992)0202.3.CO;2, 1992.

Sláma, J., Košler, J., and Condon, D. J.: Plešovice zircon-A new natural reference material for U-Pb and Hf isotopic microanalysis, Chem. Geol., 249(1–2), 1–35, https://doi.org/doi:10.1016/j.chemgeo.2007.11.005, 2008.

Söderlund, U., Patchett, P.J., Vervoort, J.D., and Isachsen, C.E.: The 176 Lu decay constant determined by Lu-Hf and U-Pb isotope systematics of Precambrian mafic intrusions, Earth. Planet. Sc. Lett., 219(3), 311–324, https://doi.org/10.1016/S0012-821X(04)00012-3, 2004.

Sun, S. S., and McDonough, W. F.: Chemical and isotopic systematics of oceanic basalts: implications for mantle composition and processes, Geol. Soc. Lond. Spec. Publ., 42, 313–345, https://doi.org/10.1144/GSL.SP.1989.042.01.19, 1989.

Tang. J., Xu. W. L., Wang. F., and Ge. W.C.: Subduction history of the Paleo-Pacific slab beneath Eurasian continent: Mesozoic-Paleogene magmatic records in Northeast Asia, Sci. China. Earth. Sci., 61, 527–559, https://doi.org/CNKI:SUN:JDXG.0.2018-05-003, 2018.

Trail, D., Watson, E. B., and Tailby, N. D.: Ce and Eu anomalies in zircon as proxies for the oxidation state of magmas, Geochim. Cosmochim. Ac., 97, 70–87, https://doi.org/10.1016/j.gca.2012.08.032, 2012.

Vervoort, J.D., and Blichert-Toft, J.: Evolution of the depleted mantle: Hf isotope evidence from juvenile rocks through time, Geochim. Cosmochim. Ac., 63(3),

533–556, https://doi.org/10.1016/S0016-7037(98)00274-9, 1999.

Wan, Y.S., Song, B., Liu, D.Y., Wilde, S. A., Wu, J.S., Shi, Y.R., Yin, X.Y., and Zhou, H.Y.: 2006. SHRIMP U-Pb zircon geochronology of Palaeoproterozoic metasedimentary rocks in the North China Craton: Evidence for a major Late Palaeoproterozoic tectonothermal event, Precambrian. Res., 149, 271, https://doi.org/10.1016/j.precamres.2006.06.006, 2006.

Wang, F., Liu, F., Schertl, H.P., Xu, W., Liu, P., and Tian, Z.: Detrital zircon U-Pb geochronology and Hf isotopes of the Liaohe Group, Jiao-Liao-Ji Belt: Implications for the Paleoproterozoic tectonic evolution, Precambrian. Res., 340, 105633, 10.1016/j.precamres.2020.105633, 2020b.

Wang, N., Wu, C. L, Lei, M., and Chen, H.J.: Petrogenesis and tectonic implications of the Early Paleozoic granites in the western segment of the North Qilian orogenic belt, China, Lithos, 312–313, 89–107, https://doi.org/10.1016/j.lithos.2018.04.023, 2018.

Wang, Q., Xu, J. F., Jian, P., Bao Z. W., Zhao. Z. H., Li. C. F., Xiong. X. L., and Ma, J. L.: Petrogenesis of adakitic porphyries in an extensional tectonic setting, Dexing, South China: Implications for the genesis of porphyry copper mineralization, J. Petrol., 47(1), 119–144, https://doi.org/10.1093/petrology/egi070, 2006.

Wang, X. P., Oh, C. W., Peng, P., Zhai, M. G., Wang, X. H., and Lee, B. Y.: Distribution pattern of age and geochemistry of 2.18-2.14 Ga I- and A-type granites and their implication for the tectonics of the Liao-Ji belt in the North China Craton, Lithos, 364–365, 105518,

1014   https://doi.org/10.1016/j.lithos.2020.105518, 2020a.

1015   Wang, X., Griffin, W. L., Chen, J., Huang, P.Y., and Li, X.: U and Th contents and

1016   Th/U ratios of zircon in felsic and mafic magmatic rocks: Improved zircon-melt

1017   distribution coefficients, Acta. Geol. Sin. Engl., 85, 164–174,

1018   https://doi.org/10.1111/j.1755-6724.2011.00387.x, 2011.

1019   Wang, X., Griffin, W. L., O'Reilly, S. Y., and Li, W.X.: Three stages of zircon growth

1020   in magmatic rocks from the Pingtan Complex, eastern China, Acta. Geol. Sin.

1021   Engl., 81, 68–80, https://doi.org/10.3321/j.issn:1000-9515.2007.01.008, 2007.

1022   Wang, X.L., Lv, X., Liu, Y.J., Zhao, Y.Y., Li, C., Wu, W.B., Wang, Y.P., and Li, H.Y.:

1023   LA-ICP-MS zircon U-Pb ages, geochemical characteristics of Late Triassic

1024   intrusives in Xiuyan area, eastern Liaoning and their geological significances, Ore.

1025   Geol. Rev., 65, 401–416, https://doi.org/10.16509/j.georeview.2019.02.010, 2019.

1026   Watson, E. B., and Harrison, T. M.: Zircon saturation revisited: temperature and

1027   composition effects in a variety of crustal magma types, Earth. Planet. Sci. Lett.,

1028   64, 295–304, https://doi.org/10.1016/0012-821X(83)90211-X, 1983.

1029   Watson, E. B., and Harrison, T. M.: Zircon thermometer reveals minimum melting

1030   conditions on earliest Earth, Science, 308, 841–844,

1031   https://doi.org/10.1126/science.1110873, 2005.

1032   Whalen, J. B., Currie, K. L., and Chappell, B. W.: A-type granites: geochemical

1033   characteristics, discrimination and petrogenesis, Contrib. Mineral. Petr., 95, 407–

1034   419, https://doi.org/10.1007/BF00402202, 1987.

1035   Wolf, M. B., and London, D.: Apatite dissolution into peraluminous haplogranitic melts:

An experimental study of solubilities and mechanisms, Geochim. Cosmochim. Acta., 58, 4127–4145. https://doi.org/10.1016/0016-7037(94)90269-0, 1994.

Wu, F. Y., Jahn, B. M., Wilde, S. A., Lo, C. H., Yui, T. F., Lin, Q., Ge, W. C., and Sun, D. Y: Highly fractionated I-type granites in NE China (I): geochronology and petrogenesis, Lithos, 66, 241–273, https://doi.org/10.1016/s0024-4937(02)00222-0, 2003.

Wu, F. Y., Liu, X. C., Ji, W. Q., Wang, J. M., and Yang, L.: Highly fractionated granites: Recognition and research, Sci. China. Earth. Sci., 60, 1201–1219, https://doi.org/10.1007/s11430-016-5139-1, 2017.

Wu, F. Y., Yang, J. H., and Liu, X. M.: Geochronological framework of the Mesozoic granitic magmatism in the Liaodong Peninsula, Northeast China (in Chinese with English abstract), Geol. J. China. Univ., 11, 305–317, 2005b.

Wu, F.Y., Han, R.H., Yang, J.H., Wilde, S. A., Zhai, M.G., and Park, S. C.: Initial constraints on the timing of granitic magmatism in North Korea using U-Pb zircon geochronology, Chem. Geol., 238, 232–248, https://doi.org/10.1016/j.chemgeo.2006.11.012, 2007.

Wu, F.Y., Lin, J.Q., Wilde, S. A., Zhang, X.O., and Yang, J.H.: Nature and significance of the Early Cretaceous giant igneous event in eastern China, Earth. Planet. Sci. Lett., 233, 103–119, https://doi.org/10.1016/j.epsl.2005.02.019, 2005c.

Wu, F.Y., Yang, J.H., Wilde, S. A., and Zhang, X.O.: Geochronology, petrogenesis and tectonic implications of Jurassic granites in the Liaodong Peninsula, NE China, Chem. Geol., 221, 127–156, https://doi.org/10.1016/j.chemgeo.2005.04.010,

2005a.

Wu, F.Y., Yang, Y.H., Xie, L.W., Yang, J.H., and Xu, P.: Hf isotopic compositions of the standard zircons and baddeleyites used in U-Pb geochronology, Chem. Geol., 234, 105–126, https://doi.org/10.1016/j.chemgeo.2006.05.003, 2006.

Xu, J. F., Shinjo, R., Defant, M. J., Wang, Q., and Rapp, R. P.: Origin of Mesozoic adakitic intrusive rocks in the Ningzhen area of east China: partial melting of delaminated lower continental crust? Geology, 30(12), 1111–1114, https://doi.org/10.1130/0091-7613(2002)0302.0.CO;2, 2002.

Xue, J. X., Liu, Z. H., Liu, J. X., Dong, X. J., Feng, F., and Lian, G. H.: Geochemistry, Geochronology, Hf isotope and Tectonic Significance of the Late Jurassic Huangdi Pluton in Xiuyan, Liaodong Penins (in Chinese with English abstract), Earth Science, 46(6), 2030–2043, https://doi.org/10.3799/dqkx.2020.008, 2020.

Xue, S., Ling, M. X., Liu, Y. L., Zhang, H., and Sun, W.D.: The genesis of early Carboniferous adakitic rocks at the southern margin of the Alxa Block, North China, Lithos, 278–281, 181–194, https://doi.org/10.1016/j.lithos.2017.01.012, 2017.

Yang, F.C., Song, Y.H., Hao, L.B., and Peng, C.: Late Jurassic SHRIMP U-Pb age and Hf isotopic characteristics of granite from the Sanjiazi Area in Liaodong and their geological significance (in Chinese with English abstract), Acta. Geol. Sin. Engl., 89, 1773–1782, 2015a.

Yang, F.C., Song, Y.H., Yang, J.L., Shen, X., and Gu, Y.C.: SHRIMP U-Pb age and geochemical characteristics of granites in Wulong-Sidaogou Gold Deposit, East

1080   Liaoning (in Chinese with English abstract), Geotectonica et Metallogenia, 42,

1081   940–954, https://doi.org/10.16539/j.ddgzyckx.2018.05.010, 2018.

1082 Yang, J. H., Wu, F. Y., Xie, L. W., and Liu, X. M.: Petrogenesis and tectonic

1083   implications of Kuangdonggou synites in the Liaodong Peninsula, east North

1084   China Craton: Constraints from in-suit zircon U-Pb ages and Hf isotopes (in

1085   Chinese with English abstract), Acta. Petrol. Sin., 23, 263–276,

1086   https://doi.org/10.1016/j.sedgeo.2006.03.028, 2007.

1087 Yang, J.H., Wu, F.Y., Lo, C.H., Chung, S.L., Zhang, Y,B., and Wilde, S.A.:

1088   Deformation age of Jurassic granites in the Dandong area, eastern China: Ar-

1089   40/Ar-39 geochronological constraints (in Chinese with English abstract), Acta.

1090   Petrol. Sin., 20(5), 1205–1214, 2004.

1091 Yang, M. C., Chen, B., and Yan, C.: Petrological, geochronological, geochemical and

1092   Sr-Nd-Hf isotopic constraints on the petrogenesis of the Shuangcha

1093   Paleoproterozoic megaporphyritic granite in the southern Jilin Province: Tectonic

1094   implications (in Chinese with English abstract), Acta. Petrol. Sin., 31, 1573–1588,

1095   2015b.

1096 Yang, M.C., Chen, B., and Yan, C.: Paleoproterozoic Gneissic Granites in the Liaoji

1097   Mobile Belt, North China Craton: Implications for Tectonic Setting. In: Zhai M.,

1098   Zhao Y., Zhao T. (eds) Main Tectonic Events and Metallogeny of the North China

1099   Craton, Springer. Geology. Springer. Singapore., 155–180,

1100   https://doi.org/10.1007/978-981-10-1064-4_7, 2016.

1101 Yu, S., Zhang, J., and Del Real, P. G.: Geochemistry and zircon U-Pb ages of adakitic

rocks from the Dulan area of the North Qaidam UHP terrane, north Tibet: constraints on the timing and nature of regional tectonothermal events associated with collisional orogeny, Gondwana. Res., 21, 167–179, https://doi.org/10.1016/j.gr.2011.07.024, 2012.

Yuan, H.L., Gao, S., Dai, M.N., Zong, C.L., Günther, D., Fontaine, G.H., Liu, X.M., and Diwu, C.R.: Simultaneous determinations of U-Pb age, Hf isotopes and trace element compositions of zircon by excimer laser-ablation quadrupole and multiple-collector ICP-MS, Chem. Geol., 247, 100–118, https://doi.org/10.1016/j.chemgeo.2007.10.003, 2008.

Yuan, L. L., Zhang, X. H., Xue, F. H., Han, C. M., Chen, H. H., and Zhai, M. G.: Two episodes of Paleoproterozoic mafic intrusions from Liaoning province, North China Craton: Petrogenesis and tectonic implications, Precambrian. Res., 264, 119–139, https://doi.org/10.1016/j.precamres.2015.04.017, 2015.

Zeng, R.Y., Lai, J.Q., Mao, X.C., Li, B., Ju, P.J., and Tao, S.L.: Geochemistry, zircon U-Pb dating and Hf isotopies composition of Paleozoic granitoids in Jinchuan, NW China: Constraints on their petrogenesis, source characteristics and tectonic implication, J. Asian. Earth. Sci., 121, 20–33, https://doi.org/10.1016/j.jseaes.2016.02.009, 2016.

Zeng, R.Y., Lai, J.Q., Mao, X.C., Li, B., Zhang, J.D., Bayless, R., and Yang, L.Z.: Paleoproterozoic Multiple Tectonothermal Events in the Longshoushan Area, Western North China Craton and Their Geological Implication: Evidence from Geochemistry, Zircon U-Pb Geochronology and Hf Isotopes, Minerals. Basel., 8,

1124 https://doi.org/10.3390/MIN8090361, 2018.

1125 Zhai, M.G., Meng, Q.R., Liu, J.M., Hou, Q.L., Hu, S.B., Li, Z., Zhang, H.F., Liu, W.,

1126 Shao, J.A., and Zhu, R.X.: Geological features of Mesozoic tectonic regime

1127 inversion in eastern North China and implication for geodynamics, Earth. Science.

1128 Frontiers., 11, 285–298, https://doi.org/10.3321/j.issn:1005-2321.2004.03.027,

1129 2004.

1130 Zhan, Q. Y., Zhu, D. C., Wang, Q., Weinberg, R. F., Xie, J. C., Li, S. M., Zhang, L.L.,

1131 and Zhao, Z. D.: Source and pressure effects in the genesis of the Late Triassic

1132 high Sr/Y granites from the Songpan-Ganzi Fold Belt, eastern Tibetan Plateau,

1133 Lithos, 368–369, https://doi.org/10.1016/j.lithos.2020.105584, 2020.

1134 Zhang, B., Guo, F., Zhang, X. B., Wu, Y.M., Wang, G.Q., and Zhao, L.: Early

1135 Cretaceous subduction of Paleo-Pacific Ocean in the coastal region of SE China:

1136 Petrological and geochemical constraints from the mafic intrusions, Lithos, 334–

1137 335, 8–24, https://doi.org/10.1016/j.lithos.2019.03.010, 2019.

1138 Zhang, Q., Qian, Q., Wang, E.Q., Wang, Y., Zhao, T.P., Hao, J., and Guo, G.J.: An

1139 East China plateau in mid-late Yanshanian period: implication from adakites,

1140 Chinese (in Chinese with English abstract). Chinese Journal of Geology, 36 (2),

1141 248–255, 2001.

1142 Zhang, Q., Wang, Y., Liu, H., and Wang, Y.: On the space-time distribution and

1143 geodynamic environments of adakites in China annex: controversies over differing

1144 opinions for adakites in China (in Chinese with English abstract), Earth Science

1145 Frontiers, https://doi.org/10.1016/S0955-2219(02)00073-0, 2003.

1146   Zhang, S., Zhu, G., Xiao, S.Y., Su, N., Liu, C., Wu, X.D., Yin, H., Li, Y.J., and Lu,

1147   Y.C.: Temporal variations in the dynamic evolution of an overriding plate:

1148   Evidence from the Wulong area in the eastern North China Craton, China, Geol.

1149   Soc. Am. Bull., 132(9–10), 2023–2042, https://doi.org/10.1130/B35465.1, 2020.

1150   Zhao, K.D., Jiang, S.Y., Ling, H.F., and Palmer, M. R.: Reliability of LA-ICP-MS U-

1151   Pb dating of zircons with high U concentrations: A case study from the U-bearing

1152   Douzhashan Granite in South China, Chem. Geol., 389, 110–121,

1153   https://doi.org/10.1016/j.chemgeo.2014.09.018, 2014.

1154   Zhao, K.D., Jiang, S.Y., Ling, H.F., and Palmer, M. R.: Reliability of LA-ICP-MS U-

1155   Pb dating of zircons with high U concentrations: A case study from the U-bearing

1156   Douzhashan Granite in South China, Chem. Geol., 389, 110–121,

1157   https://doi.org/10.1016/j.chemgeo.2014.09.018, 2014.

1158   Zheng, J.P., and Dai, H.K.: Subduction and retreating of the western Pacific plate

1159   resulted in lithospheric mantle replacement and coupled basinmountain respond in

1160   the North China Craton, Sci. China. Earth. Sci., 61, 406–424,

1161   https://doi.org/10.1007/s11430-017-9166-8, 2018.

1162   Zheng, Y.F., Xu, Z.F., Zhao, Z.F., and Dai, L.Q.: Mesozoic mafic magmatism in North

1163   China: Implications for thinning and destruction of cratonic lithosphere, Sci. China.

1164   Earth Sci., 61, 353–385, https://doi.org/10.1007/s11430-017-9160-3, 2018.

1165   Zhu, R. X., and Xu, Y. G.: The subduction of the west Pacific plate and the destruction

1166   of the North China Craton, Sci. China. Earth Sci., 62, https://doi.org/1340-1350,

1167   10.1007/s11430-018-9356-y, 2019.

Zhu, R.X., and Xu, Y.G.: The subduction of the west Pacific plate and the destruction of the North China Craton, Sci. China. Earth. Sci., 62, 1340–1350, https://doi.org/10.1007/s11430-018-9356-y, 2019.

Table captions

Table S1. Major element (wt. %) and trace element (ppm) compositions of the Zhoujiapuzi granite

Table S2. Raman microprobe data

Table S3. The zircon major element (wt. %) and trace element (ppm) from the Zhoujiapuzi granite

Table S4. Zircon La-ICP-MS U-Pb isotopic data and ages of the Zhoujiapuzi granite

Table S5. Zircon Hf isotopic data of the Zhoujiapuzi granite

Figure captions
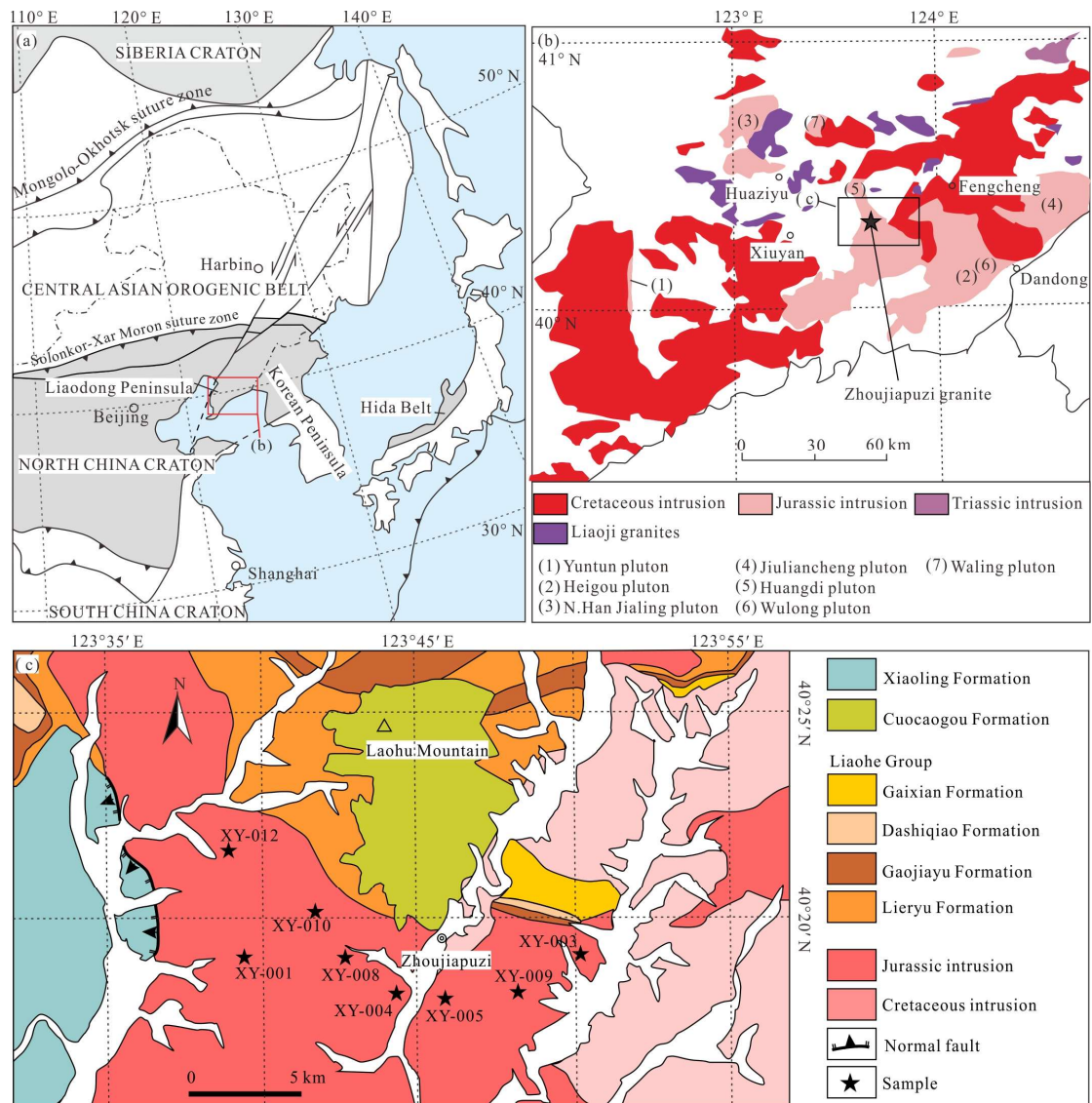
1181

Figure 1. (a) Simplified geological map of Northeast China (Modified from Li et al.,

2016); (b) distribution of Mesozoic intrusions in the Liaodong Peninsula (Modified

from Wu et al., 2005a); (c) geological map of the Zhoujiapuzi granite.

1182

1183

1184

1185
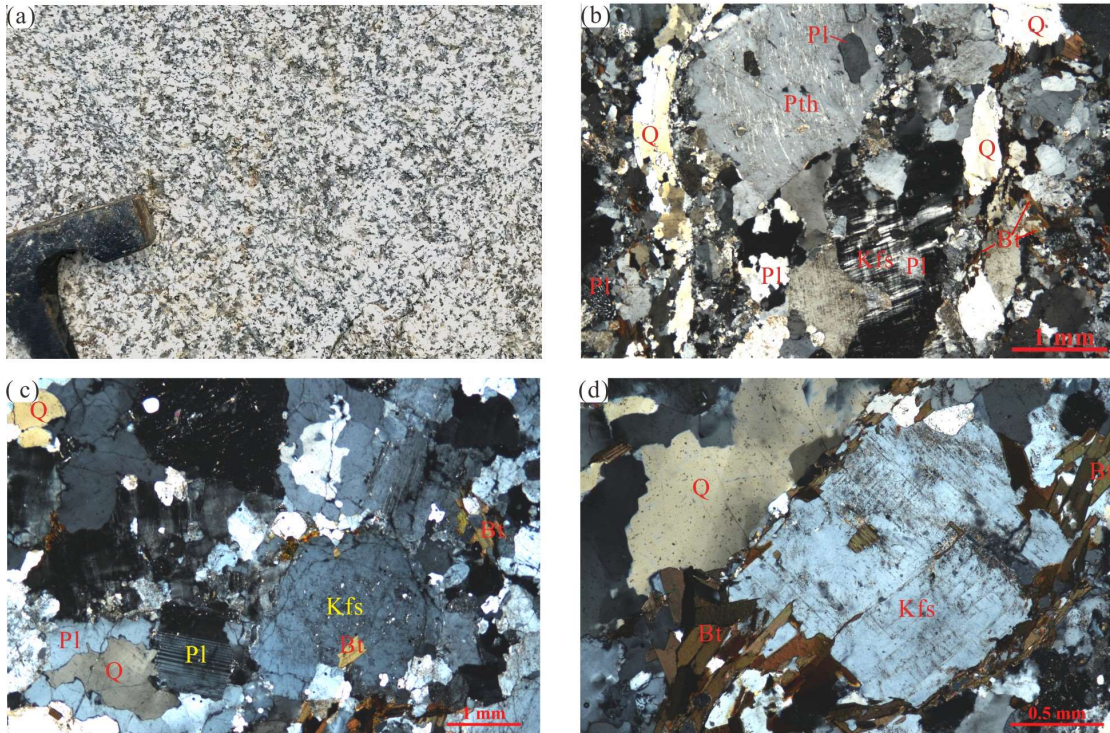
1186

1187 Figure 2. Outcrop photograph (a) and corresponding micrographs (b, c, d-

1188 perpendicular polarized light). Q quartz; Kfs feldspar; Pl plagioclase; Pth perthite; Bt

1189 biotite

1190

1191

○ Zhoujiapuzi granite (this study)
+ Other middle-late Jurassic granitoids (165−156 Ma) in Liaodong Peninsula
    (Wu et al., 2005a; Yang et al., 2015b, 2018; Xue et al., 2020)
◇ Muniuhe granitic pluton (Yang et al., 2016; Wang et al., 2020a)
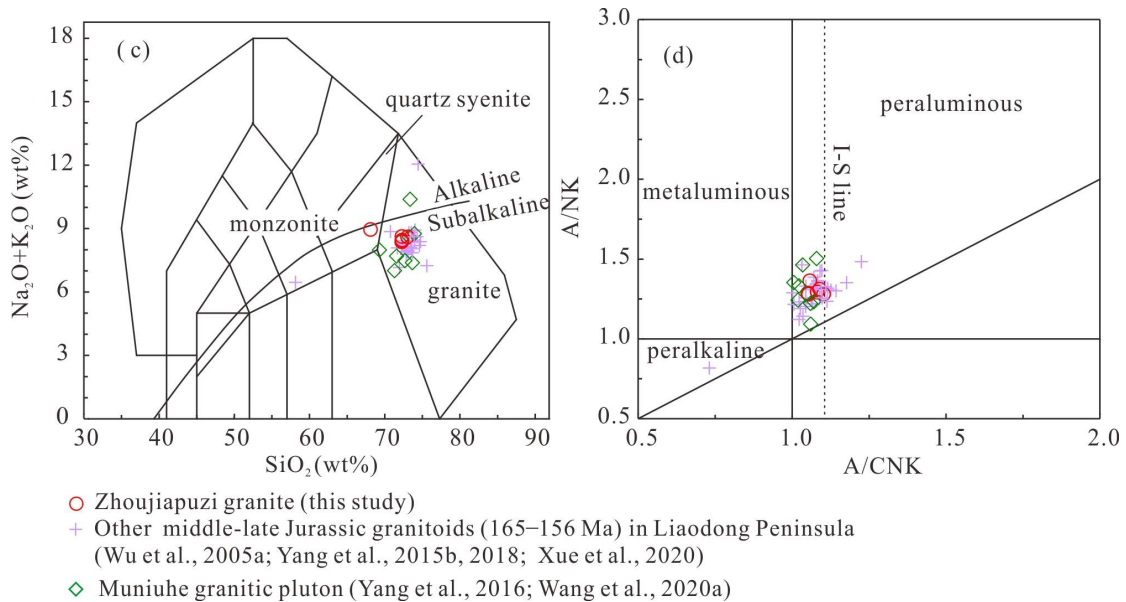
1192 Figure 3. Geochemical classification diagrams for the Zhoujiapuzi granite. (a) TAS

1193 diagram (after Frost et al.,2001); (b)A/CNK-A/NK diagram (after Maniar and

1194   Piccoli, 1989)

1195
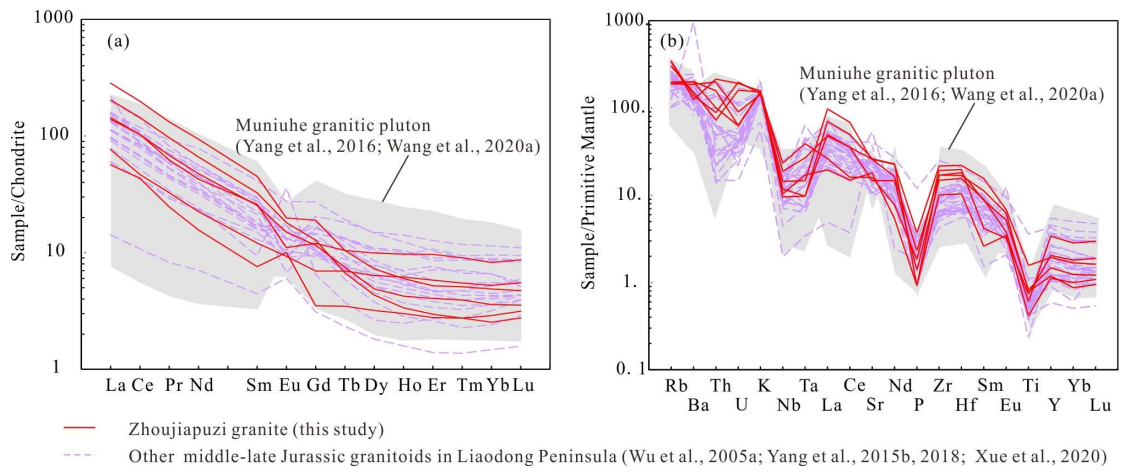
Figure 4. Chondrite-normalized REE patterns and primitive mantle-normalized trace element patterns of the Zhoujiapuzi granite (chondrite and primitive mantle values are from Sun and McDonough, 1989).

1200
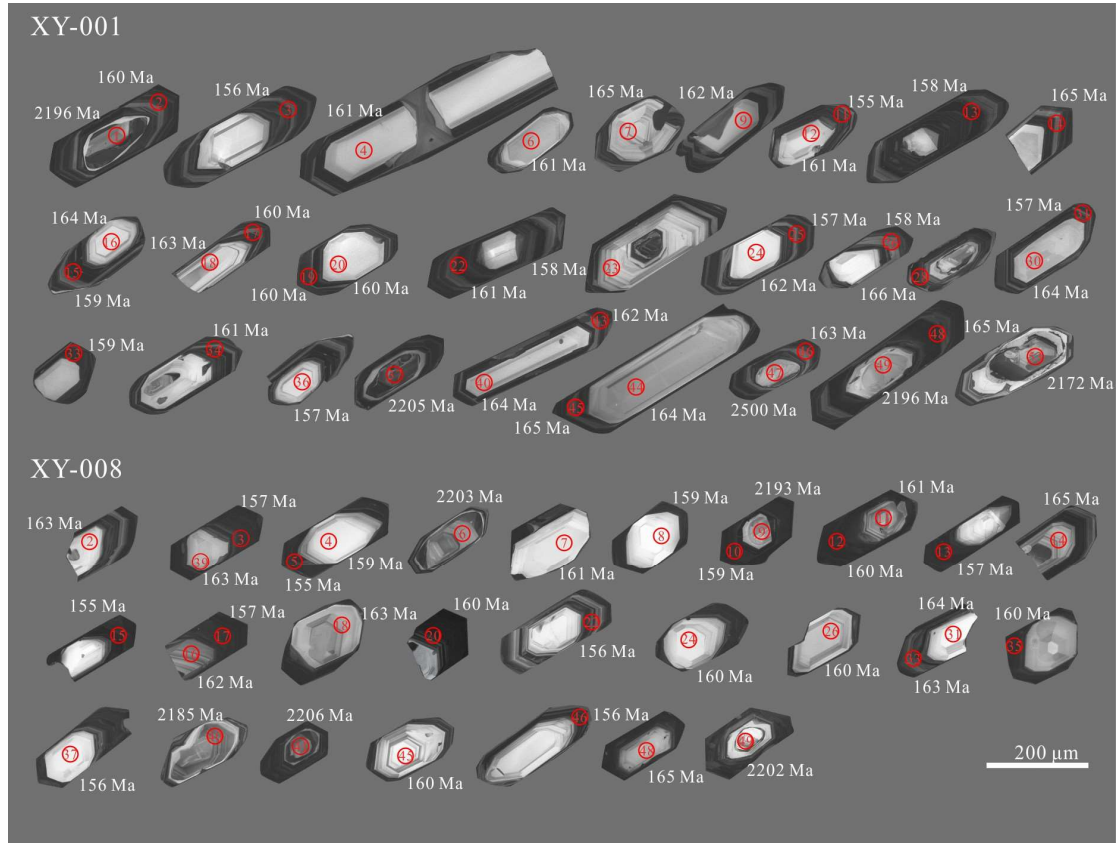
1202   Figure 5. CL images of zircons. Circles denote U-Pb analysis spot. Numbers in the

1203   circles are the spot numbers. Numbers near the analytical spots are the U–Pb ages

1204   (Ma).

1205
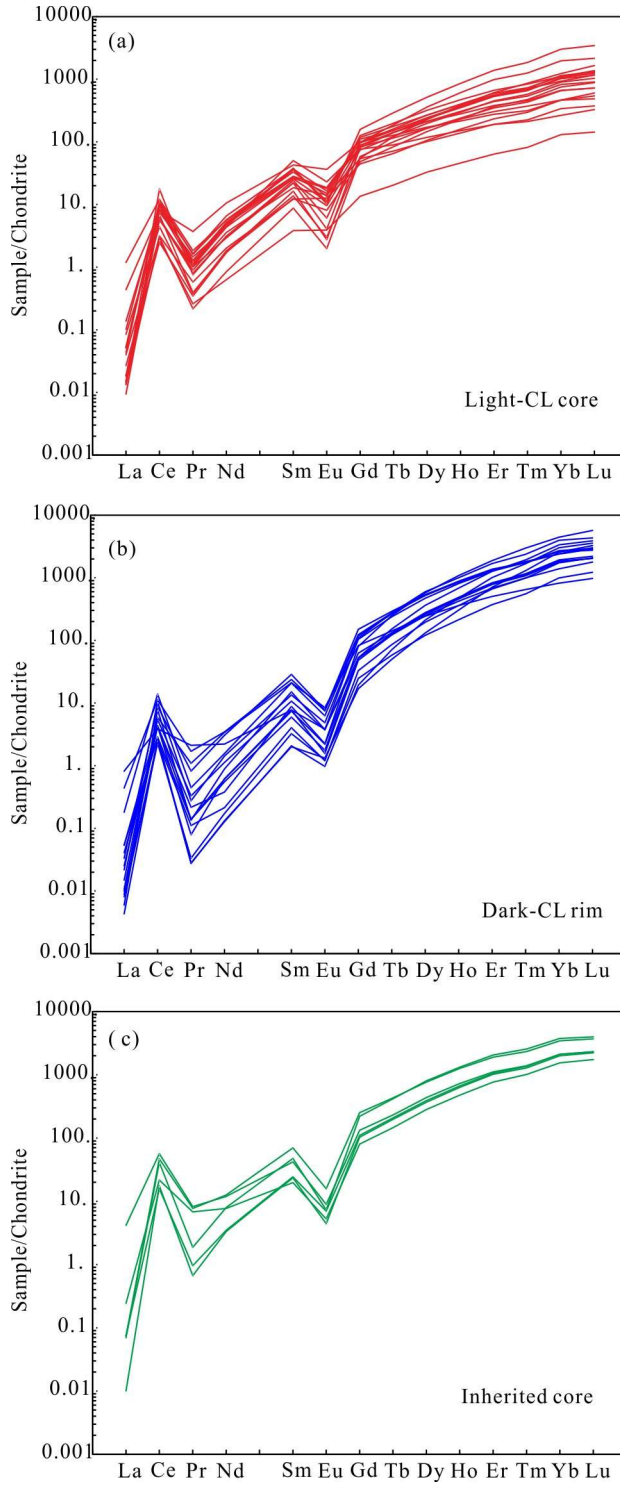
1206

1207   Figure 6. Chondrite-normalized REE patterns of zircon (chondrite values are from

1208   Sun and McDonough, 1989).

1209
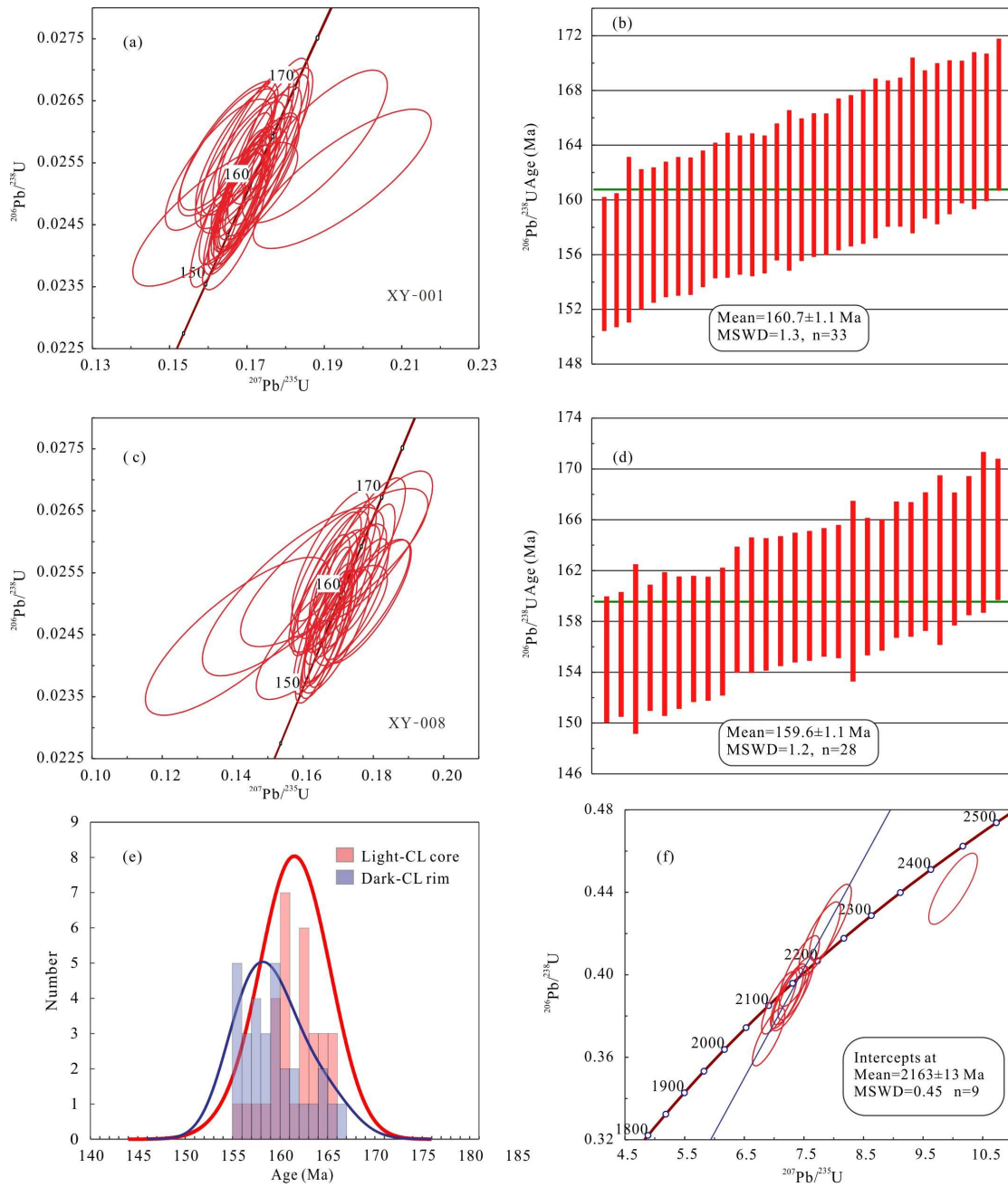
1210

1211 Figure 7. Concordia diagrams for zircon LA-ICP-MS U-Pb analyses.

1212
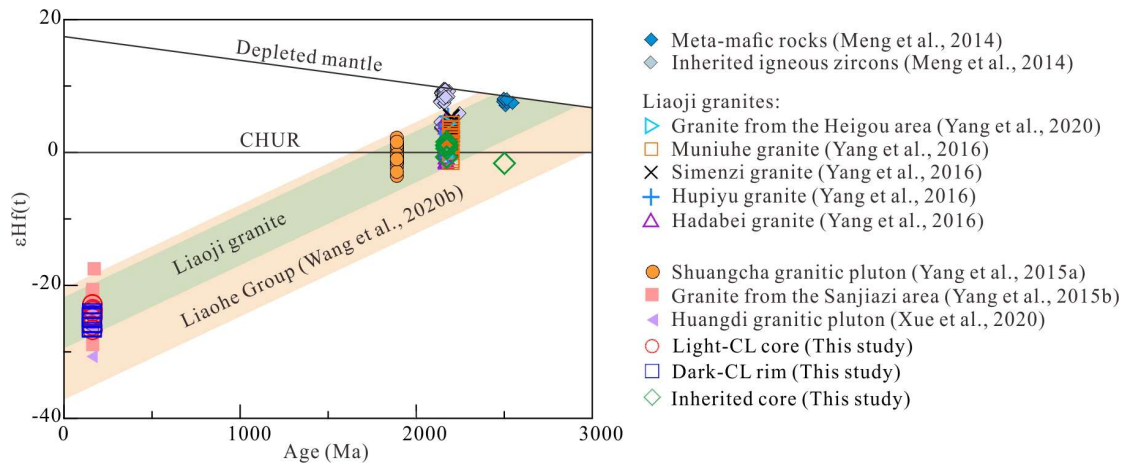
Figure 8. Zircon εHf(t)-age (Ma) diagram for samples in this study and published data

for the region.
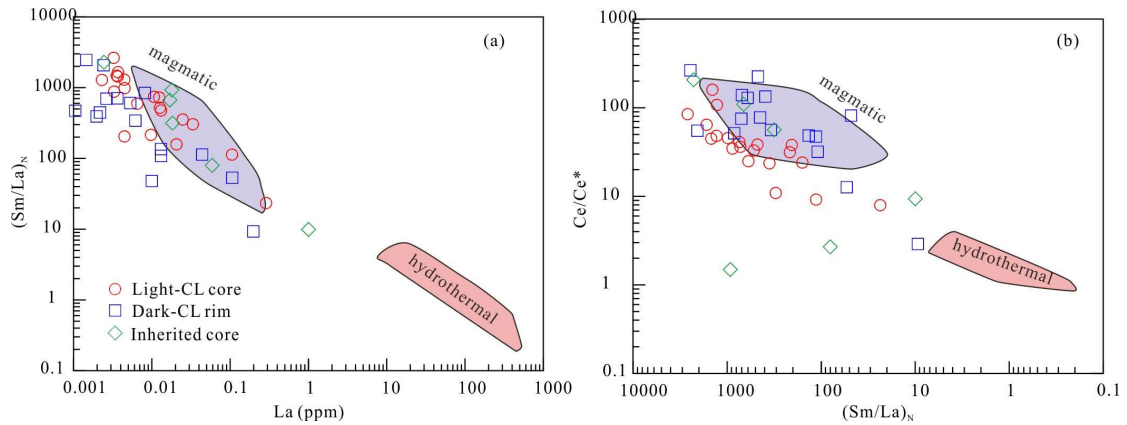
Fig. 9. Discrimination plots for magmatic and hydrothermal zircon (Hoskin, 2005).
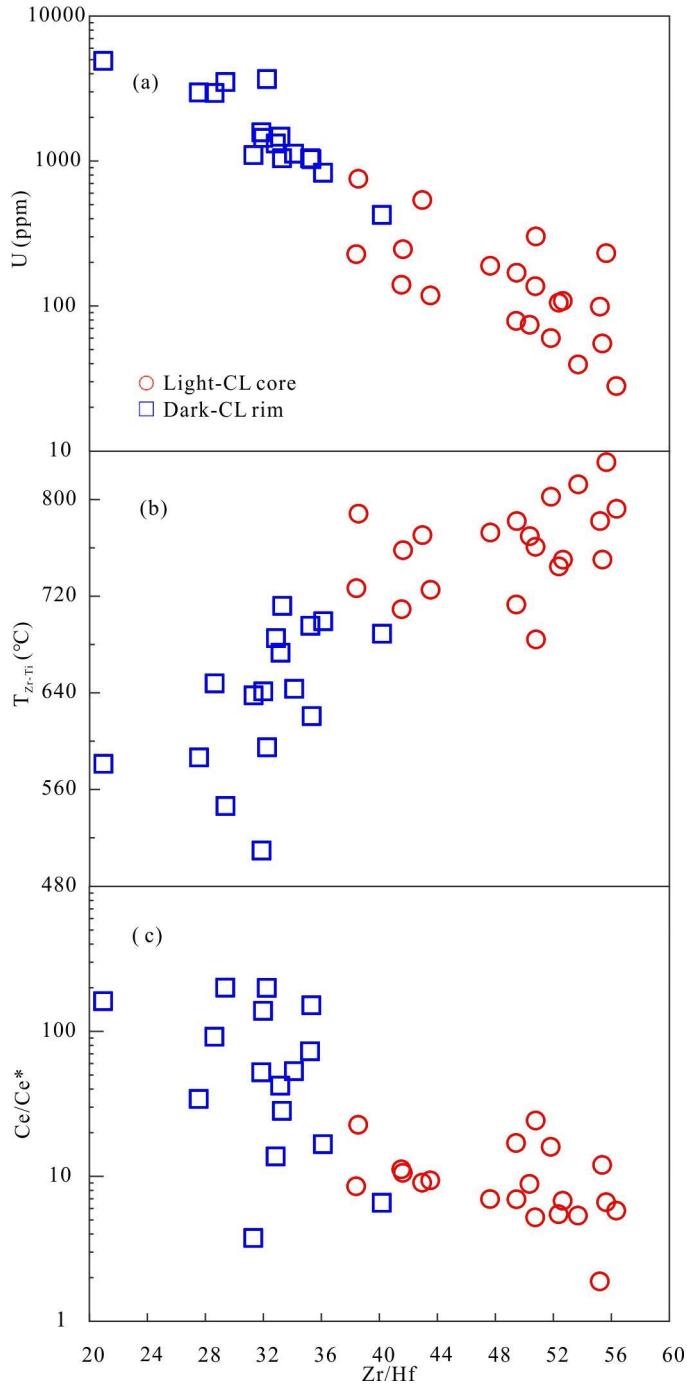
1220

1221   Figure 10. Covariation diagrams for zircon from the Zhoujiapuzi granite. (a) U vs.

1222   Zr/Hf; (b) T_{Zr-Ti} vs. Zr/Hf; (c) Ce/Ce* vs. Zr/Hf.

1223
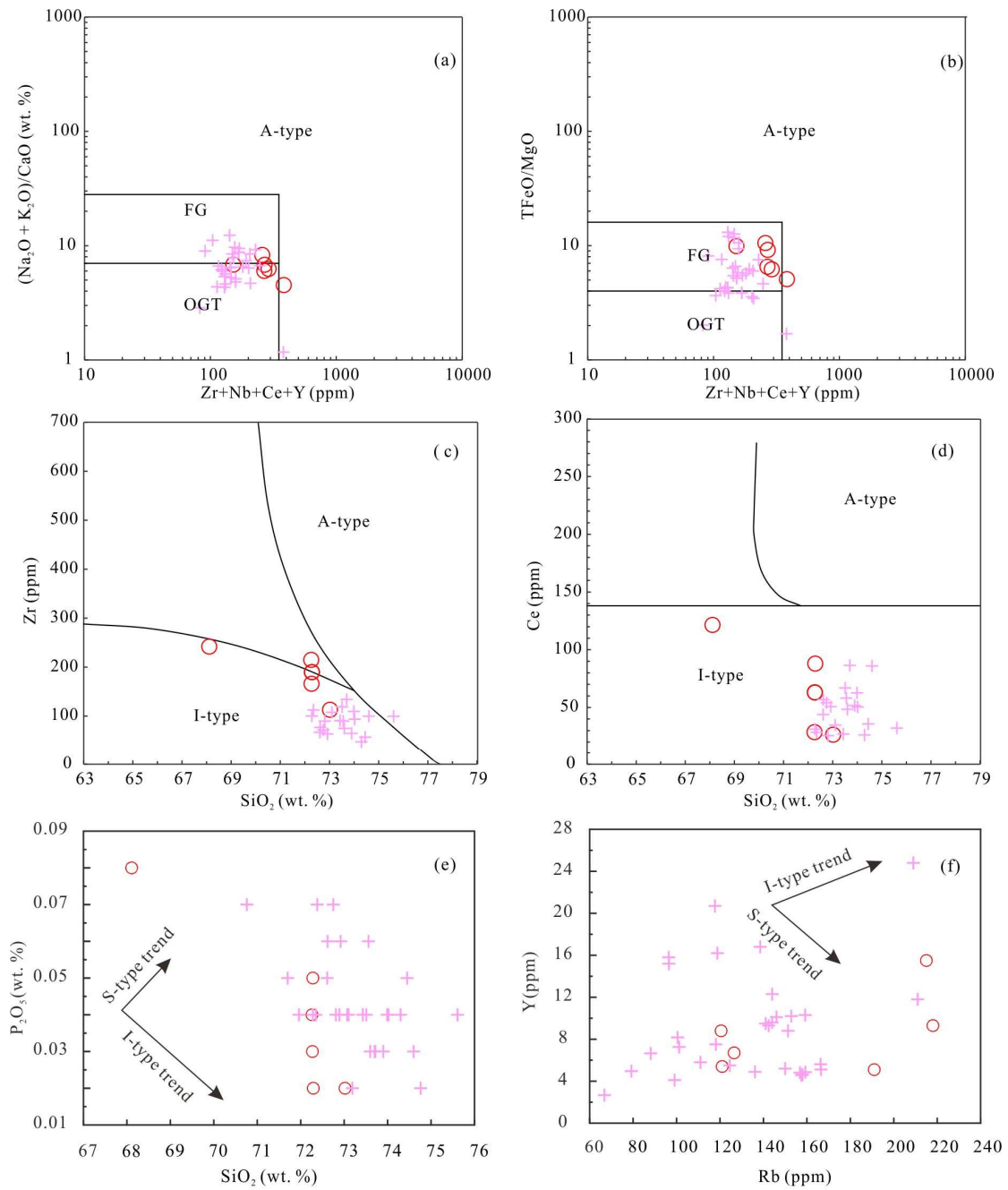
○ Zhoujiapuzi granite (this study)

+ Other middle-late Jurassic granitoids in Liaodong Peninsula (Wu et al., 2005a; Yang et al., 2015b, 2018; Xue et al., 2020)

1224

1225 Figure 11. Chemical variation diagrams for the Zhoujiapuzi granite. (a and b)

1226 Zr+Nb+Ce+Y vs. (Na$_2$O + K$_2$O)/CaO and TFeO/MgO (after Whalen et al., 1987); (c

1227 and d) SiO$_2$ vs. Zr and Ce (after Collins et al., 1982); (e) SiO$_2$ vs. P$_2$O$_5$ diagram; (f)

1228 Rb vs. Y diagram

1229
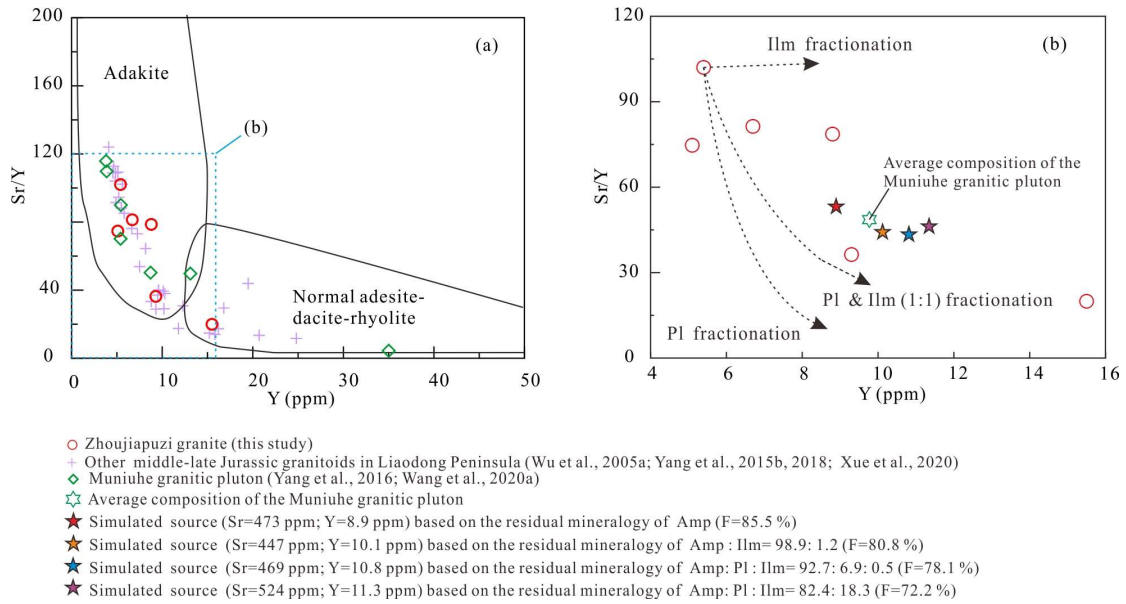
 Figure 12. Adakite discrimination diagrams for the Zhoujiapuzi granite (after Defant

 and Drummond, 1990).
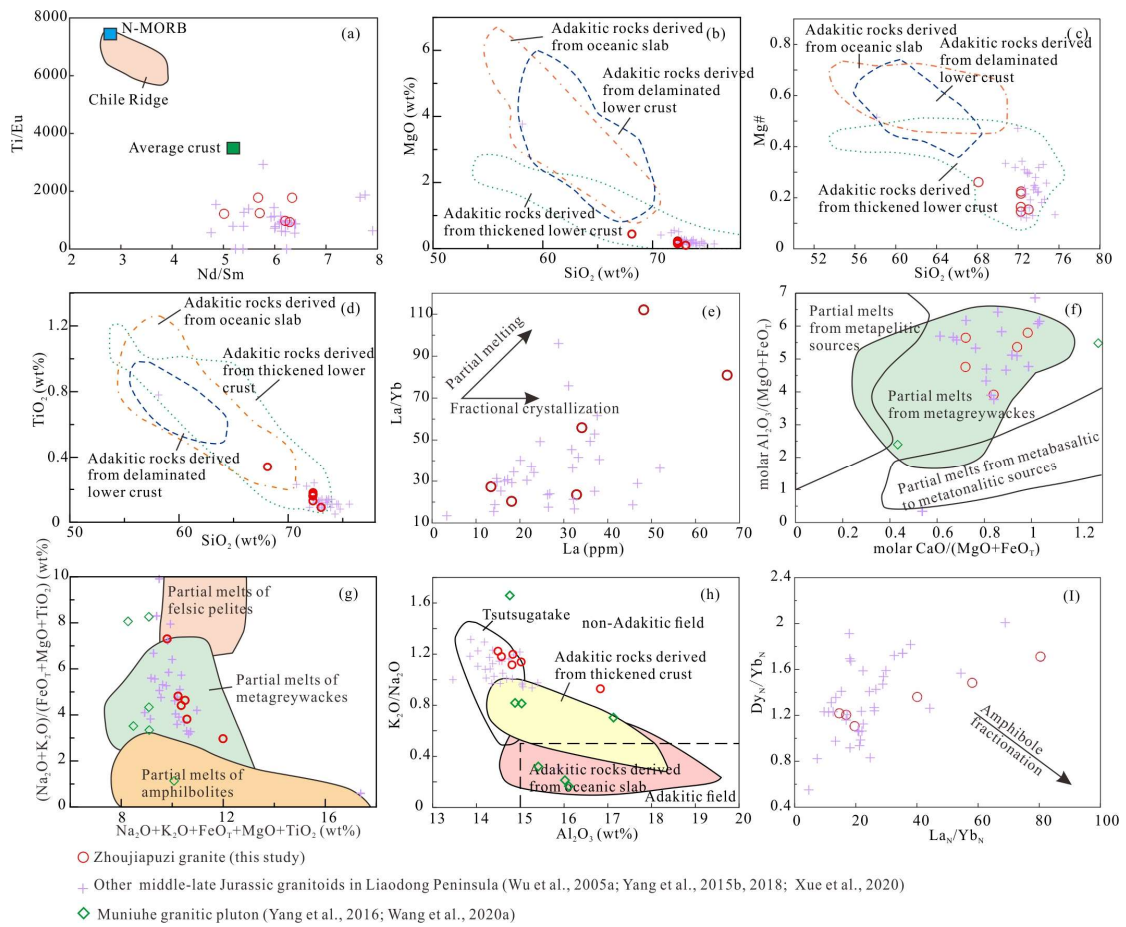
 Figure 13. Source characteristics (a-d and f-h) and crystal fractionation (e and i)

discrimination diagrams for the Zhoujiapuzi granite. Plots of (a) Nd/Sm vs. Ti/Eu (Yu et al., 2012); (b-d) SiO_2 vs. MgO, Mg# and TiO_2 (after Wang et al., 2006); (e) La vs. La/Yb (Gao et al., 2007); (f) molar $Al_2O_3/(MgO+FeO_T)$ vs. molar $CaO/(MgO+FeO_T)$ (after Altherr et al., 2000); (g) $(Na_2O+K_2O)/(FeO_T+MgO+TiO_2)$ vs. $Na_2O+K_2O+FeO_T+MgO+TiO_2$ (after Patiño Douce, 1999); (h) K_2O/Na_2O vs. Al_2O_3 diagrams (after Kamei et al., 2009); (i) La_N/Yb_N vs. Dy_N/Yb_N.
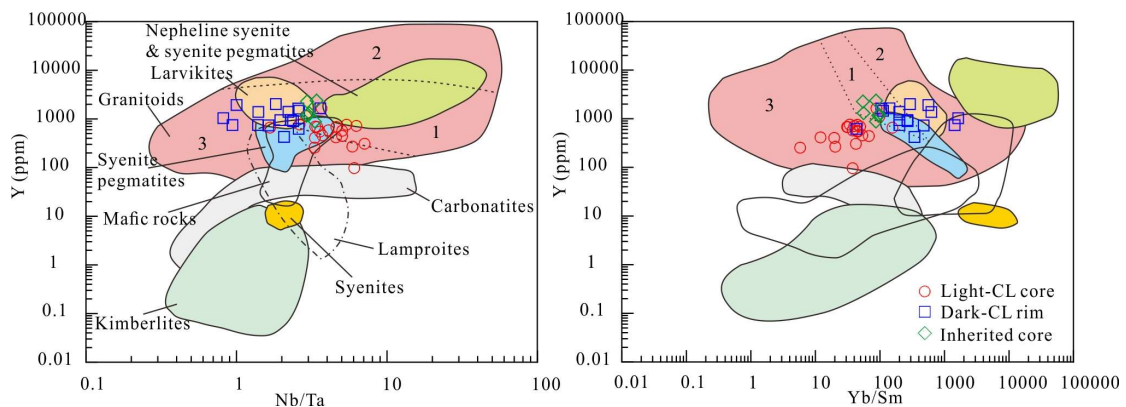
Figure 14. The fields of zircon compositions used as discriminants for different rock types (after Belousova et al., 2002). 'Granitoids' include: 1 aplites and leucogranites; 2 granites; 3 granodiorites and tonalities